10-22-2010

# A Novel Approach to X-ray Mirror Bending Stability and Control

Michael Weinbaum
*University of South Florida*

# A Novel Approach to X-ray Mirror Bending Stability and Control

by

Michael Weinbaum

A thesis submitted in partial fulfillment
of the requirements for the degree of
Master of Science of Mechanical Engineering
Department of Mechanical Engineering
College of Engineering
University of South Florida

Major Professor: Alex Volinsky, Ph.D.
Nathan Crane, Ph.D.
Delcie Durham, Ph.D.

Date of Approval:
October 22, 2010

Keywords:
Thin Films, Thermal Mismatch, Slope Error, Free Electron Laser, Uneven Heating

**Dedication**

To my wife

**Acknowledgements**

The author would like to thank Harald Sinn, Germano Gallasso, Antje Trapp, and Fan Yang and the rest of Workgroup 73 at European XFEL. Vielen Dank für euer Hilfe.

**Table of Contents**

## List of Tables

## List of Figures

## List of Equations

**Abstract**

A novel, no-contact approach to X-ray mirror bending control is presented here, proposed for use on the beamlines of the European X-ray Free Electron Laser (XFEL) project. A set of mirrors with tunable bending radii are desired, that will maintain their optical properties even as the beam incidence causes local heating. Various mechanical bending mechanisms have been proposed and used on other beamlines, which can take up a lot of physical space, demanding more vacuum power, while using expensive high precision servomotors. Rather than bend the mirror by mechanical means, it is proposed to heat the mirror to produce the desired bending. This could work two ways. One scenario calls for a finely tunable heat lamp to irradiate the back surface of the mirror while the X-ray laser heats the front side. With appropriate tuning, simulations show that this approach can keep the mirror flat, and perhaps produce a circular profile. The second scenario is similar to the first, but a thin film of tungsten is added to the back of the silicon mirror. This scenario calls for the temperature of the mirror to change homogenously to affect the desired bending, and in this case the profile should be cylindrical. In both scenarios the uneven nature of the incident radiation causes distortions that may be undesirable. Both scenarios are simulated and it is shown that the stress produced by a metal film may minimize this distortion. The response time of the mirror and configuration of both the heating and cooling mechanism are also considered.

## Ch. 1 Introduction to European XFEL

The European XFEL project in many ways can be summed up with two words: bigger and brighter. This study will ask, what are the design constraints on mirrors used in this project, and propose a design. The surface of an X-ray mirror must be almost perfectly smooth while heat originating from the X-rays themselves can cause distortions and even damage the mirror surface. This is true whether the surface is designed to be flat, curved, or toroidal. For the European XFEL project, the anticipated heat loads are orders of magnitude greater than what the previous generation of beamline components dealt with.

### *Synchrotrons and linear accelerators*

X-ray light sources, broadly, fall under two categories. The first type is a synchrotron and the second type is a linear accelerator. Both begin by injecting electrons with very high voltage into a vacuum using a klystron or similar device. The synchrotron is a circular path where magnets guide the electrons to keep them travelling in a circle and not run into walls, becoming grounded. The linear accelerator simply directs the electrons to a ground; each electron travels the path only once. Photon emission occurs as these electrons change path due to interactions with magnetic fields.

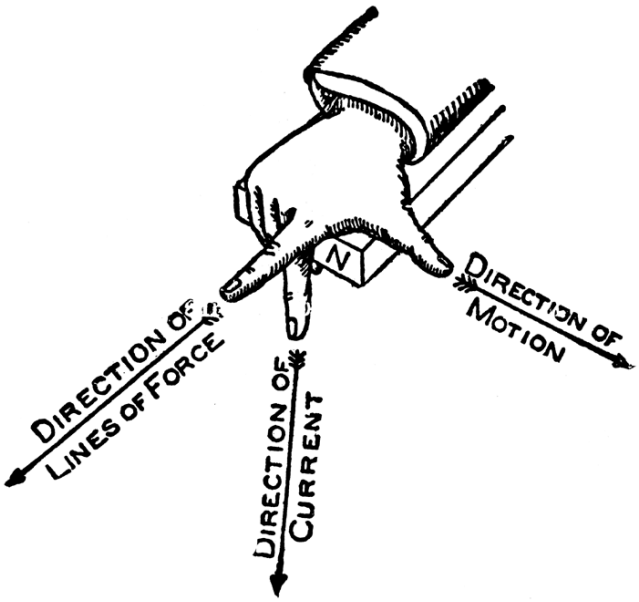


**Figure 1 – "Fleming's rule for direction of induced current. Extend the thumb, forefinger and middle finger of the right hand [as shown]. Place the hand [so that] the thumb will point in the direction in which the conductor moves, the forefinger in the direction the lines of force (N to S), then will the middle finger point in the direction in which the induced current flows."[1]**

A magnetic field will deflect any moving charged particle; the effect is similar to gravity except that the the charged particles and the field must be moving relative to each other (see Figure 1). The various magnets in a synchrotron individually steer the electrons on a hyperbolic path; multiple magnets are finely tuned along with the initial velocity of the electrons so that the electrons complete the circuit.

In the case of a linear accelerator, the electrons are typically directed to travel in-between two sets of magnets, an arrangement called an undulator, shown in Figure 2.

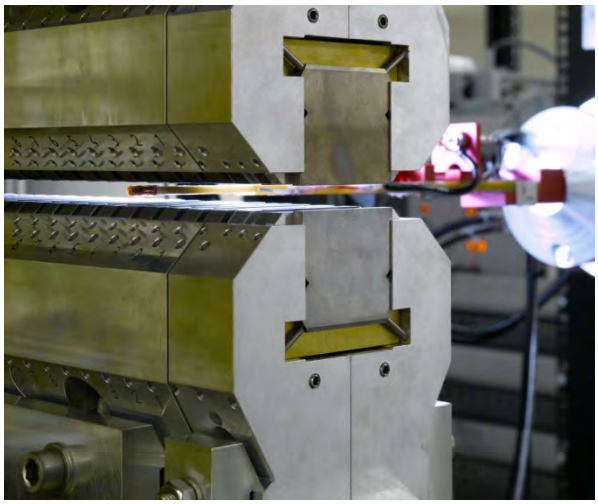

**Figure 2 -View along the beam pipe between the magnetic structure of an undulator of the storage ring PETRA III. Retrieved from DESY website and used with permission.**

These undulators force the electrons to follow a sinusoidal path along their length, with many more changes of direction in a shorter space than a typical bending magnet device. The reason the electrons are turned and twisted so much is that, whenever the magnetic field around the electron changes, not only does the acceleration on the electron change, but a photon is typically emitted. This photon's path is usually parallel to the change in acceleration, or along the radius of its curved path. In the case of linear accelerators and undulators, however, the electrons are already travelling at nearly the speed of light. This means that the emitted radiation is along the same axis as the zero of the sinusoidal path of the electron. More photons are emitted with each successive peak and trough in the electron's path, all parallel to the undulator axis, producing great intensity of radiation in a single direction. This is shown in Figure 3.

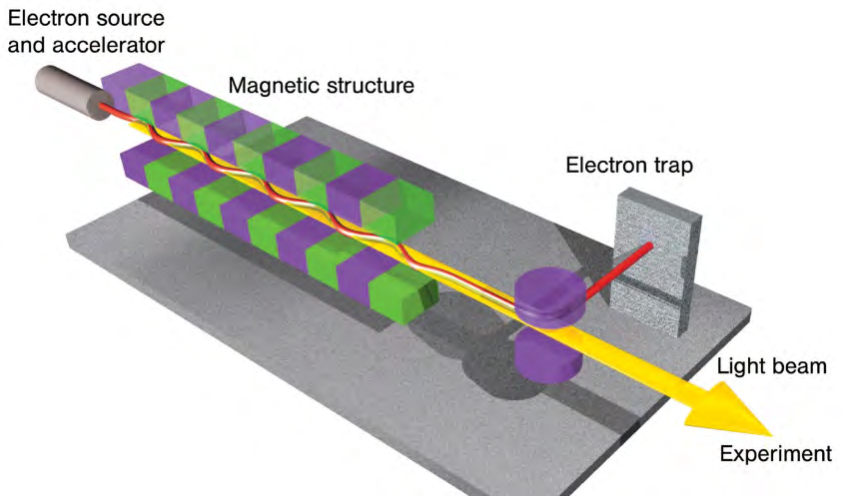


**Figure 3 - Showing path of electrons and photons in an undulator. Graphic retrieved from XFEL website and used with permission.**

The wavelength of the photons emitted, whether by a bending magnet or by an undulator, is a complex function of the kinetic energy of the electron and the magnetic field gradient; the greater either of these is, typically, the smaller the wavelength. It is unusual for such a photon to be in the visible light range, typically they range from 'high ultraviolet,' to 'hard X-ray', meaning that the range of photon energies is 10-30,000 eV. The corresponding range of wavelengths would be 10 nm down to 0.04 nm.

***X-ray free electron lasers (XFEL)***

An X-ray free electron laser (XFEL) is a special, new type of undulator-accelerator assembly where the electrons are 'entrained' into bunches by quantum mechanical effects. Existing XFEL lasers are at SPring-8 in Japan, LCLS in California, and FLASH in Hamburg. Large numbers of very high-energy electrons exit an electron gun and enter a series of cavities that each has an alternating voltage. The timing of the 'gunshot' is synchronized to the voltage phases in the cavities so that each cavity adds to the electron's electric potential as it passes. This synchronized alternating voltage

accelerates some electrons more than others, depending on their original position and velocity, and the end effect is that the electrons leave the last cavity in a 'bunch'. These bunches then travel through the undulator at nearly the speed of light, or 'high relativistic' speeds. The magnets in the undulators are tuned so that each crest and trough in the electrons' path causes photons to be emitted that have nearly the same wavelength and direction. At the end of the undulator (or series of undulators), the electrons are finally diverted by a bending magnet (this is a source of wideband radiation or spontaneous radiation) and grounded. Each electron burst now corresponds to a 'flash' of X-ray photons. The photons produced in the undulators are an 'FEL pulse'. The pulse itself is already highly monochromatic and spatially coherent, along the original path of the electrons. When the European XFEL project is complete, it is hoped that these flashes will have brilliance up to $5 \cdot 10^{33}$ (photons / s / mm$^2$ / mrad$^2$ / 0,1% bandwidth) lasting up to 100 femtoseconds. This translates to a 20 GW peak intensity (integrating the full-width half-maximum) of FEL radiation, concentrated in a small enough spot to recrystallize silicon. The time-averaged intensity is $1.6 \cdot 10^{25}$ (photons / s / mm$^2$ / mrad$^2$ / 0,1% bandwidth) and the corresponding intensity is 65 W, according to project documents[2]. Workgroup 73 has already shown that a protective diamond CVD layer, a few nanometers thick, is needed to dissipate this concentrated heat load outwards and save the single crystal mirror from re-crystallizing on the femtosecond timescale. The pauses in between pulses are so long, however, that on the millisecond timescale only the time-averaged intensity matters. This is the timescale that our steady-state and transient simulations will deal with. There is also a great amount of 'spontaneous radiation' coinciding with these pulses. The spontaneous radiation has much less coherence, both

in terms of spatial distribution and bandwidth, and must be minimized by downstream optics, for the sake of the experiments that will be done. Some of the spontaneous radiation with a lower photon energy than the FEL beam will be absorbed by solid attenuators ahead of the mirror. The mirrors will be set at an angle just shallow enough to reflect at least 90% of the photons in the FEL beam. This angle will be too shallow for the higher energy spontaneous photons and it is hoped that many of them will be absorbed by the mirror. The optical components are ultimately tasked not only with re-directing the beam away from the undulator axis for safety, but also with absorbing much of the heat loads associated with the undesired spontaneous radiation. This is especially true of the first mirror, whose position is noted in Figure 4.

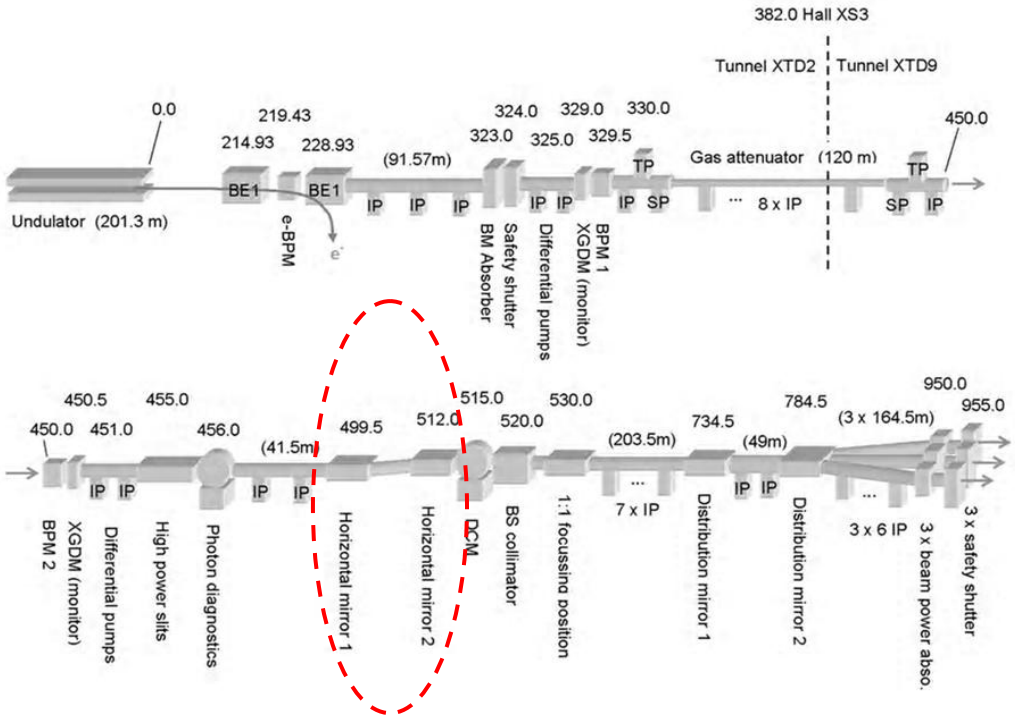


**Figure 4 - Draft of European XFEL optics from 2007, presented at Hasylab conference that year. Mirrors (circled) shown roughly 500 m away. The current design iteration for SASE 2 calls for mirror 1 to be at 260 m where heat loads will be greater[3].**

***Applications of XFEL sources***

Most of the applications of such an intense, collimated, and briefly flashing light are in the fields of biology and medicine. The amount of intensity needed to characterize a ceramic powder or metal via X-ray diffraction (XRD) is comparatively low. Repetitions in the crystal pattern of these materials selectively diffract different X-rays, and the total intensity of the diffraction pattern is typically similar to the original intensity of the source X-rays. Proteins, on the other hand, are much larger molecules, and therefore have larger gaps between the repetitions in their crystal patterns, if they even crystallize at all.

It is hoped that an XFEL beam will be able to capture useful data about the structure of such a protein from a single pulse interacting with a single complex molecule, giving off diffractions many orders of magnitude smaller than the original beam intensity. The same logic suggests that an XFEL beam may be useful to see the steps of a catalyzed biological reaction; again on a molecule-by-molecule, pulse-by-pulse basis[4].

The properties of the FEL radiation (its intensity and wavelength) will be controlled primarily by the undulator magnets' spacing. This spacing could be as small as 6 mm and each setting corresponds to unique values of intensity and wavelength for the FEL radiation, as well as unique values for the spontaneous radiation. The other controlled parameter in this vicinity will be the shutters; they will be opened the minimum amount so that the FEL beam is transmitted while as much as possible of the spontaneous radiation, which is not spatially coherent, is absorbed by the shutter blades.

***Silicon as a mirror material***

Reflectivity is a complex property. It is the fraction of the light incident on a surface that is reflected back by the surface at the 'reflected angle,' as shown in Figure 5.

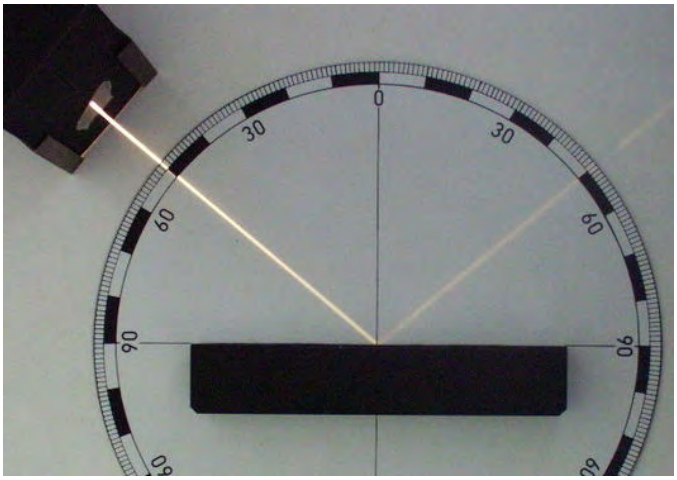


**Figure 5 - Photo explaining angle of reflection. By Zátonyi Sándor (ifj.), posted on Wikimedia under a free public license.**

The fraction cannot be greater than one without violating the First Law of Thermodynamics. Reflectivity is highly dependent on surface conditions; the smoother a surface is, the more it reflects, up to some maximum that depends on the material of the mirror itself, the incident angle, and the wavelength of the photons. Most materials are actually quite poor reflectors in the low wavelength 'high ultraviolet' to 'hard X-ray' range; though as with visible light metals are still better reflectors than non-metals. Most materials, metal or non-metal, will only reflect X-rays at very low angles of incidence, on the order of tens of milliradians (mrad). The theoretical reflectivity of any material at a 0 angle is 1; because it can be said that the photons are not interacting with the surface at all. As the angle of incidence is increased, the X-ray reflectivity of most materials trends to zero; the photons are absorbed or transmitted rather than reflected. However at small angles the reflection can be nearly complete. Mirrors designed for low-angle reflection

are also sometimes called total reflection mirrors. The greater the energy of the photon, or smaller its wavelength, the smaller the range of angles that will reflect that photon for a given material will be. For each material and incident wavelength, there is also a 'critical angle' below which (if 0 is taken as parallel to the reflecting surface) no transmission occurs, only reflection and absorption.

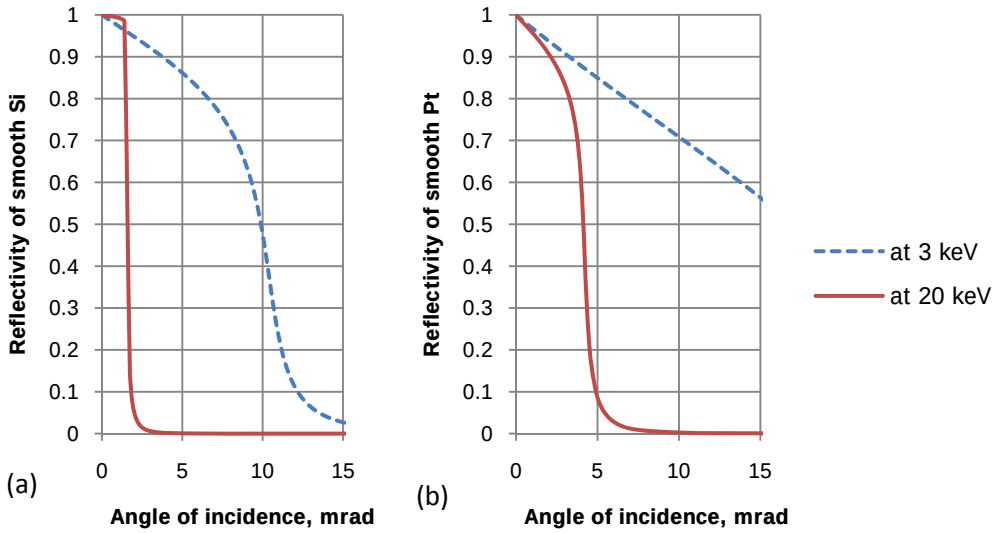


**Figure 6 – Sample Reflectivity curves of (a) Silicon and (b) Platinum. Higher energy X-rays are reflected by a smaller range of angles. Data from http://henke.lbl.gov/optical_constants/**

Even though metals are better reflectors than non-metals, silicon is the dominant substrate for X-ray mirrors at these types of facilities. This is because of the surface quality required. Random surface roughness much greater than 2 nm can greatly decrease the surface reflectivity in the hard X-ray regime[5]. This type of perfection is very difficult to achieve in anything but a single crystal material. In single crystal silicon, roughness less than 0.5 nm is feasible[6]. Pieces of metal the size of an X-ray mirror cannot match single crystal silicon in terms of dimensional stability. Machining a

polycrystalline piece of metal often reveals voids and relieves complex stress patterns so that no matter how many times the 'perfect' tool passes, roughness is still there. Single crystal metals are not as available as single crystal silicon. This is because of semiconductor industry developments.

The front surface of silicon mirrors is often coated with platinum by chemical vapor deposition or a similar process, creating a smooth and stress free surface that would not have been possible out of solid, polycrystalline platinum. A platinum coated silicon mirror is more versatile, as shown in Figure 6; it maintains reflection at higher incidence angles. Platinum is one example; tungsten and nickel have very comparable reflectivity and lower cost, though obviously both have a greater tendency to oxidize, potentially compromising their optical properties. Platinum and palladium coatings are often 'primed' with chromium to improve their bond strength, other metals need no priming. These coatings are made for optical qualities only and are typically less than a micron thick; too small to change the elastic or thermal conduction properties of the mirror significantly. This paper will explore adding a metal film thick enough to bend the mirror but will not be interested in the possible small changes to heat conduction caused by the film.

***CVD coating process for silicon mirrors***

A metal film is typically added to a silicon mirror by chemical vapor deposition, or CVD. The competing process is PVD, physical vapor deposition. The CVD process involves comparatively little heat. It typically involves the mixing of a powder and a liquid or gas that will create a chemical reaction on the surface. The chemical reaction creates a free metal ion that will tend to attach to the surface, gaining electrons in the

process. The other products of the reaction, which are gases or liquids, are carried away by fans or pumps. Though noxious gases are often produced, newer methods allow the reaction to take place under a hood, not necessarily under high vacuum. However, earlier methods did require high vacuum because they were very sensitive to water vapor[7]. PVD processes more frequently require a vacuum and, depending on the metal being deposited, are generally more costly. Some metals such as aluminum and copper have chemistries that make CVD difficult to achieve so in this case PVD is preferred. A CVD process typically takes place near room temperature, and can be finished surprisingly fast; in the case of nickel, a metal film may be deposited on a surface at a rate of 250 microns per hour[8]. Nickel was the first metal to be deposited via CVD and Nickel CVD is still one of the least costly CVD processes. Its low heat and electrical conductivity make it a poor choice for semiconductors but it may be a good choice here.

The main reason CVD of metal is used on silicon is to create a small layer of electrically conductive material on top of the semiconductor which is then used to create an integrated circuit. A concern when attempting metal CVD on silicon is the formation of metal silicides (analogous to an intermetallic phase; their properties are more like a ceramic) at the interface boundary. The presence of metal silicides is problematic for two reasons; one is that the change in crystal structure may induce high stress, some deformation, and even fracture/delamination as they form. For instance, the large stresses created by molybdenum silicide formation under a molybdenum film were studied recently by Volinsky et al[9]. Another problem, for most users, is that these silicides are electrical insulators. Though silicides are stable at room temperature, their formation only becomes thermodynamically favorable at elevated temperatures. Silicide

formation typically has a starting temperature and an ending temperature. If the piece is held above the starting temperature, silicides form (with a slow rate and faster as the temperature increases) and they typically remain stable after the temperature is lowered. The 'ending' temperature for a certain silicide chemistry, say $M_2Si$, often corresponds to the 'begining' temperature for the formation of a different silicide, perhaps MSi. Silicide formation is not a concern, therefore, as long as the designer knows that the part will not be subjected to temperatures at or above the lowest possible reaction temperature. The lowest reaction temperature for nickel-silicon, for instance, is 300 °C[10], while for tungsten this value is higher, about 650 °C[11]. Avoiding that threshold should not be a problem in this case.

***Deformation due to localized heating***

Most materials, when heated evenly, will expand isotropically and this is called positive thermal strain. However, if only a small part of the solid is heated while the rest remains the same temperature, the heated portion will be under compressive stress while the neighboring portions at the lower temperature will be under tensile stress. This means that a temperature gradient whose sign never changes will typically produce a stress gradient (and the attendant shear stress) whose sign does change. The heated portion will grow less than would be dictated by its thermal expansion, while the unheated portion will grow more. The thermal conduction of the material and the resulting temperature distribution must be understood in detail before the deformation can be predicted; it will be much more difficult to get a steep temperature gradient (and therefore a steep stress gradient) on a material with high thermal conductivity and a large

characteristic thickness. Understanding deformation due to uneven heating rapidly becomes a question for either empirical study or finite elements analysis.

Recently, the heating of X-ray mirrors and its effect on mirror shape was studied by Yuan et al at Berkeley Labs[12], who attempted to minimize these effects with a Peltier cooling device attached not to the mirror but to its support. The problem as they describe it is that the mirror, when heated evenly, will also heat the aluminum support below it. The aluminum will expand more than the silicon, creating some extra stress in the mirror and unacceptable slope errors. The aluminum support has a ten times greater thermal expansion coefficient than the silicon. So the approach was to add a cooler which would keep the aluminum support at a constant temperature over a range of possible mirror temperatures. Their setup was successful in that changes to the mirror curvature no as a function of mirror temperature were greatly reduced. However, their tests were conducted in a special thermally insulated box without uneven heating from an X-ray beam, and they acknowledge that such in-situ heating would be a source of additional slope error without quantifying this.

***Curvature and bending***

Bending is a specific type of elastic deformation typical to beams. A beam is any object that is much longer than it is wide or deep, and is typically supported only intermittently along its length. The interaction between the loads, including the beam's own weight, and the supports creates a deflected shape. These deflected shapes can be described by singularity equations or other methods, but this is beyond the scope of this paper. Whether a deflected shape follows a $4^{th}$ order polynomial, or is sinusoidal, or something else entirely, at every point this deflected shape has a derivative and therefore

an instantaneous radius of curvature. An interesting consequence of the curvature along the length of the beam is that all four surfaces of the beam are also distorted- even if the beam was square and isotropic to begin with.

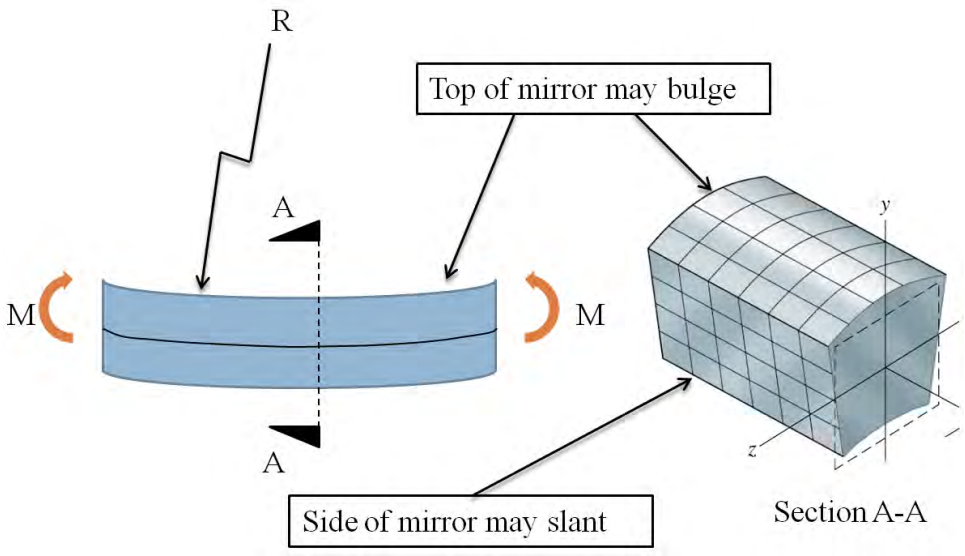


**Figure 7 - Explaining Anticlastic Bending**

When a beam bends, the inner face of the beam is compressed, its length is reduced, while the outer surface expands. The Poisson effect dictates that an infinitesimal volume under uniaxial stress will actually deflect in all three directions. If the uniaxial stress is compressive, the volume will compress in that direction but 'bulge' or expand in the other two directions. The net effect is that the overall volume, the distorted length * width * height, is nearly preserved (and exactly preserved in the case of an ideal material whose Poisson ratio is 0.5). The inner face of the beam is in compression, so this face will bulge while the outer face will 'shrink' or be 'sucked in'. The faces on the side will be slanted as shown in Figure 7.

***Warping***

The previous discussion of bending dealt with a hypothetical beam that had a square cross-section. While all four faces of the beam were distorted in different directions, the deflected shape had a plane of symmetry. This is because the loads and supports were all in that plane, and the undistorted beam was symmetric about it as well. The original square cross section of the beam has four lines of symmetry. On the other hand, the channel section shown in Figure 8 has only one line of symmetry, the horizontal line. For this reason it will twist out of plane as it bends, unless a) the load is through the shear center**,** shown in the picture, or b) all loads vectors are in to the plane of symmetry.

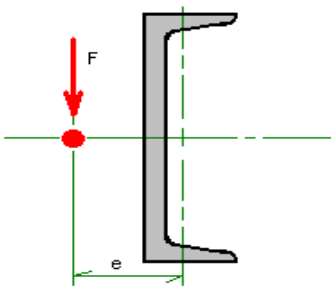


**Figure 8 - Showing the Shear Center of a typical channel section. If the line of the load is not through the shear center, warping is expected.**

This is counter-intuitive because the shear center is not even on the part itself, so it is difficult to load the beam there. Channel sections are often paired when they are expected to handle a bending load in their strong axis- the load center ideally being between the two channels, corresponding to the shear center of each. If the sections are not paired and the warping is instead constrained by a redundant member, this may introduce secondary stresses that the designer must account for.

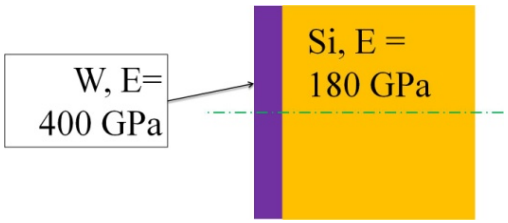


**Figure 9 – Differences in elastic modulus between a film and a substrate may create warping, if the load and supports are not along the line of symmetry shown. This representation is simplistic because single crystal silicon is anisotropic.**

Like the channel section, a mirror with a film also only has one line of symmetry, even though its rectangular shape still seems to have two lines of symmetry. Instead it is the mismatch between the Young's moduli which can create some warping, whether the original bending deformation is from internal or external forces.

***Stress, strain and bending with thin films***

Stresses in a thin film are known to cause bending deflection in the substrate, though the substrate is much larger than the film. In 1909 Stoney quantified the relationship between the film stress and the bending in a rectangular beam that this stress may cause. His equations take many forms, but in our case the source of the film stress is a temperature change working with a mismatch in thermal expansion coefficients between the film and the substrate (thermal mismatch for short). Equation 1 is Stoney's equation derived for this case and solved for the resulting bending radius.

$$r = \frac{E_s(t_s)^2\left[\frac{1-\nu_f}{E_f} + \frac{4t_f(1-\nu_s)}{t_s E_s}\right]}{6t_f(1-\nu_s)(\alpha_f - \alpha_s)(\Delta T)}$$

**Equation 1- Stoney's Equation solved for bending radius due to thermal mismatch**

It is taken from lecture notes presented by William Nix at Stanford University and available online[13]. This equation relates film thickness ($t_f$), substrate thickness ($t_s$), along with the elastic properties of both ($E_f$, $\nu_f$; $E_s$, $\nu_s$ ) and the thermal mismatch ($\alpha_f - \alpha_s$) and temperature change to find the radius of curvature of the bent shape.

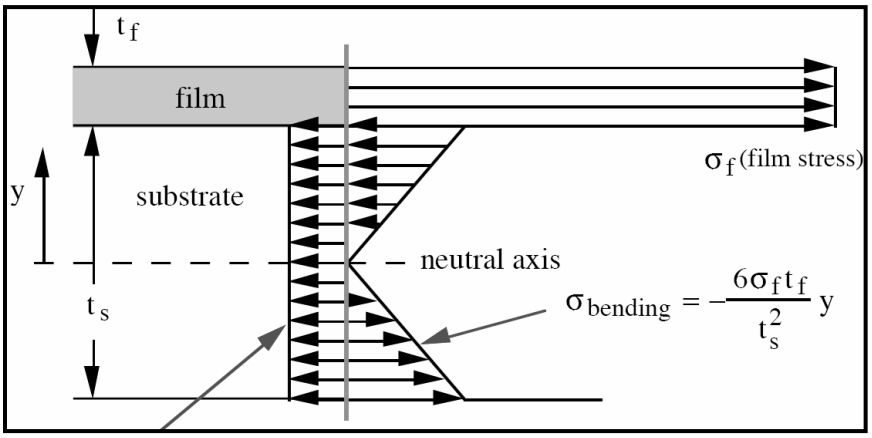


**Figure 10 – taken from the notes of Prof. W. Nix, used with permission**

Another use of Stoney's equation is to predict the tensile stress in the film itself given the same inputs:

$$\sigma_f = \frac{(\alpha_s - \alpha_f)(\Delta T)}{\frac{1-\nu_f}{E_f} + \left[\frac{1-\nu_s}{E_s} * \frac{4t_f}{t_s}\right]}$$

**Equation 2- Stress in the thin film due to thermal mismatch.**

The shear stress between the film and the substrate is related to this value, it is

$$\tau_{f-s} = \sigma_f \left[1 + \frac{4t_f}{t_s}\right]$$

**Equation 3- Shear stress between film and substrate as a function of film tensile stress**

These three equations will be used in the following section in conjunction with ANSYS simulation to validate design proposals incorporating a thin film.

***Cooling and support of existing silicon mirrors***

*"Three spheres" support*

Some recommend supporting the mirror on top of three pins with spherical heads. These pins ideally are only able to return force directly up, and would balance the mirror as a tripod does. This support scheme would be non-redundant. The disadvantage is that no part of the support can fail without the mirror falling. The advantage is that stress caused by misfit parts is eliminated, though bending stress and deflection are often greater in a non-redundant support scheme than a redundant one. The stress state is predictable using a simpler set of equations without needing to take the deflected shape into account. The spheres should also have less friction than a flat or cylindrical support, reducing (but not eliminating) the likelihood of axial load on the mirror due to a change in temperature.

If we imagine a mirror that, in the absence of gravity, is completely flat, we know that this mirror will bend when placed on the three spheres support; it will sag. This may create optical distortions. For this reason, when the mirror surface is polished with elastic emission machining, the mirror is already sitting on its support, if it was intended to be supported this way. If the supports are moved, the mirror may sag in a different way and need to be polished again.

*Cylinder bender*

The most common way to compensate for the sag that results from non-redundant support is to add precisely controlled bending actuators to the mirror support scheme. This takes the form of three or four cylinders in contact with the flat surface of the mirror,

two on one side and the remaining one or two on the other. The cylinders are only allowed to move in one direction and the position of the cylinders is changed with nanometer or even Angstrom precision. This precision is typically achieved using stepper motors and stiff levers. The actuators are typically separated from the ultra high vacuum chamber by bellows. The line of contact between the mirror and the cylinder may have a large stress concentration which must be understood and monitored.

*Epoxy leaf spring bender*

There are at least two X-ray mirror set-ups, one in Berkeley and one in Stanford, which support the mirror vertically on solid metal while allowing it to be bent by attaching leaf springs to the mirror's ends with epoxy. The load on the leaf spring, and therefore the bending radius of the mirror, can be changed by much less precise stepper motors than were required for the cylinder bender while using epoxy rather than compressive contact produces less stress concentrations. The large solid contact area can also be useful for cooling. Such an arrangement is also called a u-bender.

*Indium-Gallium bath*

Indium-Gallium amalgams are sometimes liquid at room temperature (the Eutectic temperature being lower than both pure metal melting points) and much less toxic than mercury. They are already used in some applications as a low temperature solder and are finding use as a thermal conductor in the liquid state. The X28C beamline at Case Western Reserve University employs a silicon mirror with no rigid support; it is placed in a stainless steel 'bathtub' and liquid Indalloy 51 metal is carefully poured around it, eventually causing the mirror to float. The density of Indalloy 51 is roughly

three times greater than the density of silicon; for this reason the lower third of the mirror becomes unusable, unless the 'bobber mechanism' the authors mention is employed[14].

In spite of these difficulties, the advantages of a liquid support are great. No stress concentration is imposed and there is no need to worry about the variable properties of cured adhesive. Also, the Prandtl number of a liquid metal is exceptionally low compared to other fluids.

$$\mathrm{Pr} = \frac{\nu}{\alpha} = \frac{\text{viscous diffusion rate}}{\text{thermal diffusion rate}} = \frac{c_p \mu}{k}$$

**Equation 4 – The Prandtl number is a unitless ratio. Image from Wikipedia.**

**Table 1- Prandtl numbers of selected liquids**

| Liquid | Prandtl number |
|---|---|
| Mercury | ~0.015 |
| R-12 | ~4.5 |
| Water | ~7 |

Whether the mirror actually floats in liquid metal or is simply coated with it, because of the low Prandtl number we can assume that the liquid bath has a negligible temperature gradient and no need to force flow. This means that the surfaces wetted by liquid metal can be assumed to have constant temperature, which simplifies analysis.

*Liquid metal channels*

While a liquid metal bath would cool the bottom surface of a silicon mirror, for a mirror aligned vertically it may be important to cool the top surface as well. One approach is to 'paint' the top surface with liquid metal and place a cooled copper plate

(typically with internal channels for chilled water) on top of that. Another approach is to machine or otherwise fabricate one or more trenches into the top surface, which a copper fin will fit into, and fill the gap with liquid metal. The fin in turn would be brazed or soldered to a copper pipe carrying cold water. Such a setup was proposed by Fermé at Société Européenne de Systèmes Optiques[15]. It may be significantly less expensive and challenging than a liquid metal bath

*Cooled copper plate*

Many silicon mirrors end up being attached to a copper plate with channels inside for water or another cooling fluid. A leading manufacturer of such plates is SESO in France. These plates can be manufactured to nearly the flatness requirements of the mirrors they support. They are typically quite thick and it is commonly practiced to place only a small layer of single crystal silicon on top of them, perhaps 1 cm thick, with an epoxy adhesive. 20 kW cooling power is claimed for a typical 1 m long X-ray mirror[16]. In applications where thermal mismatch may be a concern, the mirror may simply rest on a cooled copper plate with a liquid contact, perhaps oil or even liquid metal, carefully spread.

## Ch. 2 Design constraints of mirrors in the European XFEL

The purpose of the primary mirrors in the European XFEL project is to allow the experiment site to be off-axis from the path the electrons would take if the final bending magnet failed. Though each mirror can only change the path of the X-ray radiation slightly due to the low angle of reflection, with enough distance between the mirrors a 5 m beam displacement is created. The heat load on the second mirror in the pair will be less than that on the first mirror in the pair, so design will focus on the first mirror. There are two beamlines under consideration, SASE 1 and SASE 2. SASE stands for Self-Amplified Spontaneous Emission The goal is for one type of mirror to perform sufficiently in both beamlines.

### *Length, height, and flatness*

The following relies heavily on the April 14th draft version of "Conceptual Design of X-ray Beam Lines" by Work Group Package 73 members. The mirror will reflect in its vertical plane, displacing the beam horizontally. A second mirror will return the beam back to its original angle. The distribution of photons in the FEL beam is Gaussian along two planes. If a significant number of photons does not hit the mirror surface, and instead hits the edge because the mirror is undersized, an interference pattern will develop. The further downstream the mirrors are, the wider the Gaussian distribution becomes; this is a linear relationship defined by the 'angle of divergence'. With the

photons more spread out, the concentrated heat load associated with absorption becomes easier to deal with. However, the mirror must be bigger. In particular, it must be longer due to the very low angles of incidence of less than 8 mrad, depending on the wavelength setting. The low angle stretches the beam footprint. Working group 73 has settled on a set of parameters that will require the face of the mirror to be 80 cm long, 5 cm tall. The size requirement derives from the configuration of SASE 1, where the mirror is 435 m away from the undulators and the beam spread, for this reason, is wider. However, the heat load will be more intense in the SASE 2 beamline than it is in the SASE 1. The first mirror is 260 m away in the case of SASE 2. The more concentrated heat load of SASE 2 will therefore be used for our simulations. The total distance from the end of the undulator to the experiment site in both cases is over 900 meters.

Kazuto Yamauchi et al from Japan Synchrotron Radiation Research Institute recently quantified the way small bumps on a silicon mirror will distort an FEL beam[17]. The bumps were imagined as randomly placed bell-curves (Gaussian bumps) of various heights and spreads along the length, and a raytracing finite simulator, integrating the Fresnel-Kresnel integral, was employed. It was found that the spread of a bump is not very important, but the height of the bump is important. With X-ray frequencies, the researchers found that 2 nm height is an important cutoff point in terms of beam quality. Unacceptable distortions, in the form of diffraction peaks, become likely beyond this point. For this reason, $\leq 2$ nm flatness seems to be an adequate design goal for this study. This is achievable from a manufacturing standpoint. Using elastic emission machining, Mimura et al at SPring-8 report that surface roughness down to 0.2 nm RMS is achievable over a length of 96 mm[18]. Therefore, 2 nm RMS roughness

over 80 cm seems to be an easier task. However, the bumps studied here originate not from machining problems but due to heating. Because the bumps created by FEL radiation may not be ideal, Gaussian bumps, the deflected shape found via simulation should be examined by numerically integrating the Fresnel-Kirchhoff integral of the deflected shape after this study is complete, as long as the result is bumps within the same order of magnitude as 2 nm.

***Heat load***

The latest draft of the Workgroup 73 document proposes that the mirrors will be in front of the double crystal monochromator and behind tungsten slits and a solid attenuator. The attenuator is not specified at this point, but it is likely to be an aluminum or beryllium window. An aluminum or beryllium window will absorb all of the spontaneous radiation below a certain photon energy, as shown in Figure 11, allowing only 'hard' X-rays to pass.

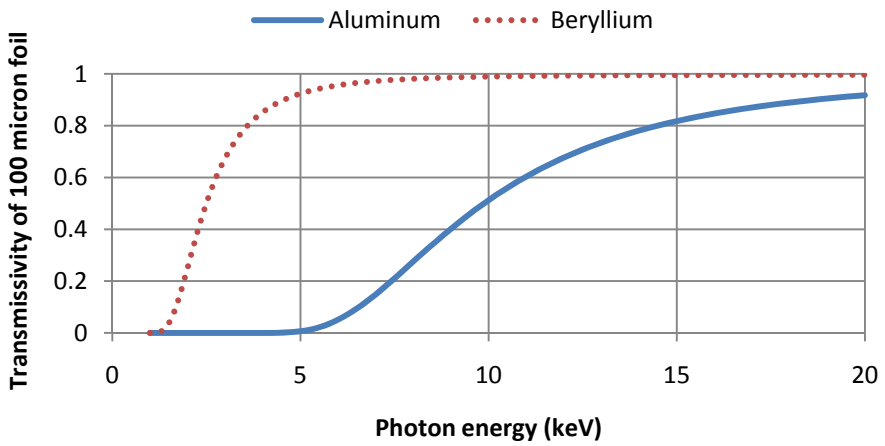


**Figure 11- Comparing the X-ray transmission of Aluminum and Beryllium, angle of incidence = 90°. Data from [http://henke.lbl.gov/optical_constants/](http://henke.lbl.gov/optical_constants/)**

At least 90% of the X-ray photons incident on the first mirror will be reflected, that is, the mirror angle will be set so that the reflectivity is at least 0.9 for the FEL radiation. The other 10% or less will be absorbed by the silicon atoms and converted into heat. A larger heat load will come from the spontaneous radiation above the FEL bandwidth that was not affected by the attenuator, most of it will be absorbed by the mirror. The heat reaction is a matter of individual photons being absorbed by individual atoms. Microscopically, the process at work is heat generation varying with respect to position. It is not like absorption of thermal radiation which is a surface phenomenon. The rate of photon absorption is proportional to the percentage of unabsorbed photons remaining, so that the 'slice' closest to the surface absorbs more photons, and has a greater heat load than all the slices below it. This is a case of exponential decay, shown below.

$$\boldsymbol{G(z) = G_0 * e^{-z/l}}$$

**Equation 5- Exponential decay of X-ray intensity as photons are absorbed by atoms**

$G_0$ is the rate of photon absorption/heat generation at the surface and *l* is the 'absorption length' which is a function of the wavelength and the size of the atoms absorbing the radiation. In the case of smaller nuclei or shorter wavelengths, the average X-ray photon may pass many layers of atoms before finally being absorbed and the absorption length is longer. In the case of larger nuclei or longer wavelengths, 99% of the photons may be absorbed in the first few nanometers, and the absorption length is shorter. The absorption length can vary but for our purposes, since we are doing a Finite Elements simulation of the entire mirror, the length will always be small enough that over 99% of the absorbed energy will be absorbed by the nodes along the face of the mirror.

The incident radiation and the heat load will also vary along the length and width of the mirror. While the spontaneous radiation will be nearly evenly distributed over the mirror, the paths of the photons in the laser radiation are all very close together and very close to being parallel. This property of laser light is called spatial coherence. However, all the photons do not have the *exact* same path; it is more correct to say that the paths are very tightly distributed around a mean path. The distribution is normal, and the standard deviation is small. This is called a Gaussian distribution along the two axes x and y.

$$H(x,y) = \frac{H_0}{2\pi * \omega_x * \omega_y} * e^{\left(\frac{-x^2}{\omega_x{}^2} + \frac{-y^2}{\omega_y{}^2}\right)}$$

**Equation 6- Two Dimensional Gaussian Distribution of photons in FEL beam**

H is the peak intensity of the FEL beam in $W/m^2$. If the radiation were hitting the mirror head on at a $90^o$ angle of incidence, $\omega_x$ and $\omega_y$ would be equal. $\omega$ is the standard deviation, and it is in units of length. At $\omega$ away from the y-axis, the local intensity will be reduced by 63%, at $2\omega$ away the reduction is 98%, etc. The y-axis of the mirror and the path of the beam make a plane that is perpendicular to the flat face of the mirror, so the beam's footprint on the mirror is not stretched or compressed in this direction. On the other hand, the x-axis of the mirror and the mean path of the beam make a plane that intersects the mirror face at the x-axis itself, at a very shallow angle. For this reason, the beam spread in the x-direction will be much wider,

$$\omega_a = \omega_b / sin\,(\theta)$$

**Equation 7- Beam spread from the perspective of the slanted mirror**

$\theta$ is the incident angle on the mirror. $\theta$ will be less than 0.5° or 8 milliradians, so the sine of this angle is equal to the angle itself, in radians. $\omega_b$ is a property that depends

on the undulator gap setting, and the shutter gap setting. Its value also grows linearly with the distance between the undulator and the mirror. Workgroup 73 has suggested a value of 5 mm be used for $\omega_b$ in all simulations. We now have enough information to know what the heat generated in a finite volume will be with respect to position in the mirror. This function is below, where S is the intensity of the spontaneous radiation in $W/m^2$.

$$\boldsymbol{I(x,y,z) = G(z) * (S + H(x,y))}$$

**Equation 8- Intensity of FEL and spontaneous photons absorbed as a function of position**

The total heat load on the mirror is the volumetric integral of this function. These functions accurately describe the real heat load in terms of space, but not in time. The actual X-ray laser will have many intense pulses lasting less than a picosecond each, with microseconds in between of no photon flux. However, for the purposes of this study it is sufficient to consider the steady state condition of the mirror while the laser is active, and therefore only the average heat load on the mirror is interesting.

The total 'spontaneous' heat load due to the S term is 31.5 W, while the total 'laser' heat load with a Gaussian distribution is 6.5 W.

***Bending requirements***

A mirror may be bent in the interest of focusing or defocusing the FEL radiation, to spread the photons out over a larger area, or to compress the photons so that the beam size at the source is the same as the beam size at the experiment site, in spite of divergence. These are both theoretical concerns. In real applications, mirror imperfections, even in costly silicon mirrors, can destroy desired optical features.

Precisely bending the mirror can compensate for these imperfections, so that the 'bent' mirror is straightened. While systems to do this with many actuators along the mirror length are feasible and have been proposed, it is more common to see three and four point bending mechanisms being used. When bending a mirror, 'slope error' becomes an important figure of merit. To find this figure, first the desired, circular slope is defined as a function along the length of the mirror. Then the actual slope of the mirror surface is measured, again as a function along the length of the mirror, and the two are subtracted from each other, giving an error function that also varies with respect to the length. It is generally acceptable for slope error to be 3 microradians (μrad) or less[19]. This is not expected to be different for FEL beams. A mechanical bending mechanism is often a source, rather than a remedy, of slope error. Only the center section of a beam in 4-point bending has a constant radius; no part of a beam in 3-point bending has a constant radius. However, because the radii of focus are often so large that the deflection is on the order of microns, these mechanical benders often give sufficient performance. The European XFEL Work Group Package 73 has requested that any bending mechanism be able to precisely go from flat to a radius of 20 km for the purposes of focusing. An ability to curve even beyond 20 km, down to 10 km would be desired but not required. The bending only needs to take place in a single axis, giving a cylindrical, rather than toroidal, profile.

## Ch. 3 Description, simulation, and analysis of proposed designs

The following chapter lists five possible designs for the mirror, each with an added bit of complexity compared to the one that came before. The first design was proposed by others, and the next four are proposed improvements. Each of these proposals are considered in terms of the deflected mirror shape resulting from them, and these shapes are simulated without considering gravity or the support arrangement, as if the mirror were floating in space. Deflections caused by gravity and the support scheme will add to the deflection caused by a thermal gradient, and both can be minimized or controlled separately. The last section of this chapter proposes how to support the mirror.

### *Remote cooling*

The first instinct of the engineers designing the European XFEL optics was to cool the mirrors remotely, that is by radiation only. Because the presence of air or other gas will tend to attenuate and scatter X-rays, external convection was out of question for this component. The hope was that by bringing a cold (100 K via a pulse tube refrigerator), black plate near to the front surface, the mirror would be adequately cooled by near-blackbody thermal radiation exchange. The plate could be moved away when not needed so that the mean temperature of the mirror would remain constant.

The good thing about this approach is that the hot spot of the front of the mirror becomes sandwiched between two cold spots created by the cold plate. Since the average temperature of the front and back surfaces of the mirror are the same, this minimizes

bending along the axis, though bending (outwards, towards the beam source) still occurs. The magnitude of the bending is small, with the high point about 30 nm above the low point, and the radius of curvature is 3000 km- flat for most practical purposes. However it was found that cooling the remote plate down to 100 K would not be cost-effective for the rate of heat removal that could have achieved. A deficiency of this analysis was that the heat generation was idealized as occurring homogenously along a strip going down the front of the beam; in reality the generation will be greatest in the middle and decay with a Gaussian relation along the length and height of the face of the mirror. We will show that a heat concentration in the center can have an outsized effect on the bending radius. So, while the beginning design constraint was 'don't touch the mirror', this was loosened so that the mirror was imagined as having a liquid metal contact, which will not be affected by the vacuum nor put stress on the mirror, on at least one surface. Not only does this allow the maximum heat removal rate to increase, this decision also simplifies design analysis because the surface with liquid metal can be idealized as having a homogenous temperature.

***Liquid metal cooling on a single surface***

Since the beam is intended to be reflected horizontally, the plane of the mirror is vertical. The mirror will either rest on its cooling surface, or the cooler rest on the mirror. For this reason the main heat flow, and therefore the likely alignment of the bending, is at 45° to the face of the mirror.

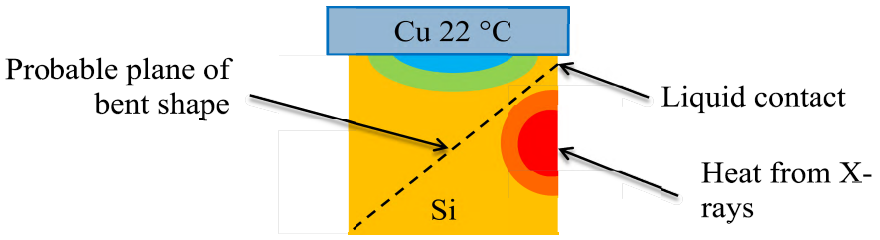


**Figure 12 – Describing one fixed-temperature surface and no other intervention. Cooled surface may also be on the bottom, mirror assumed weightless.**

This means that the mirror will want to bend both towards the beam source and either up or down, away from the cooler, as well. The bending towards the beam source is not likely to be useful, because it will spread, rather than focus the beam. The bending up or down will tend to slant the reflecting surface due to anticlastic effects. Even though this setup is unlikely to give a useful mirror, we will simulate it for the sake of comparison; a control group.

To complete the simulation, a 4 * 5 * 80 $cm^3$ solid silicon bar is described in ANSYS Workbench. The x-axis is 'up and down' while the z-axis is 'towards or away from the beam source'. The y-axis is 'along the length of the mirror'. The x, y, and z axes are shown on Figure 13 and the other figures from ANSYS Workbench. The 4 cm depth is chosen so the mirror will more easily bend in the desired z-axis rather than up and down (in the x axis by this simulation). The initial temperature is 22 °C and the top surface is also held at 22 °C. The center of the optical face of the mirror is the origin of the coordinate system in ANSYS, which is also the center of the Gaussian heat load. The mesh maximum edge length is initially set at 5 mm but this had to be relaxed to 1 cm for the computing power available. The larger mesh size had a minimal effect on the results. The mirror is divided into elements that are each rectangular prisms like the mirror itself. ANSYS APDL is used to describe the *I(x,y,z)* function for the heat load, and this function

is brought into Workbench as a command. First, the steady-state thermal application runs, and the *I(x,y,z)* function is checked by verifying that the correct amount of heat, about 38 W, leaves the cooled surface. The temperature distribution is also examined, to make sure that a Gaussian 'hot spot' appears, Figure 13. Next, the steady-state structural application runs with no loads or supports to find the 'floating in space' deflected shape in response to the temperature change. The results, showing bending in two axes, are Figure 14. Finally, a log of the steady-state structural results may be made and brought back into ANSYS APDL so the deflected shape can be examined in more detail.

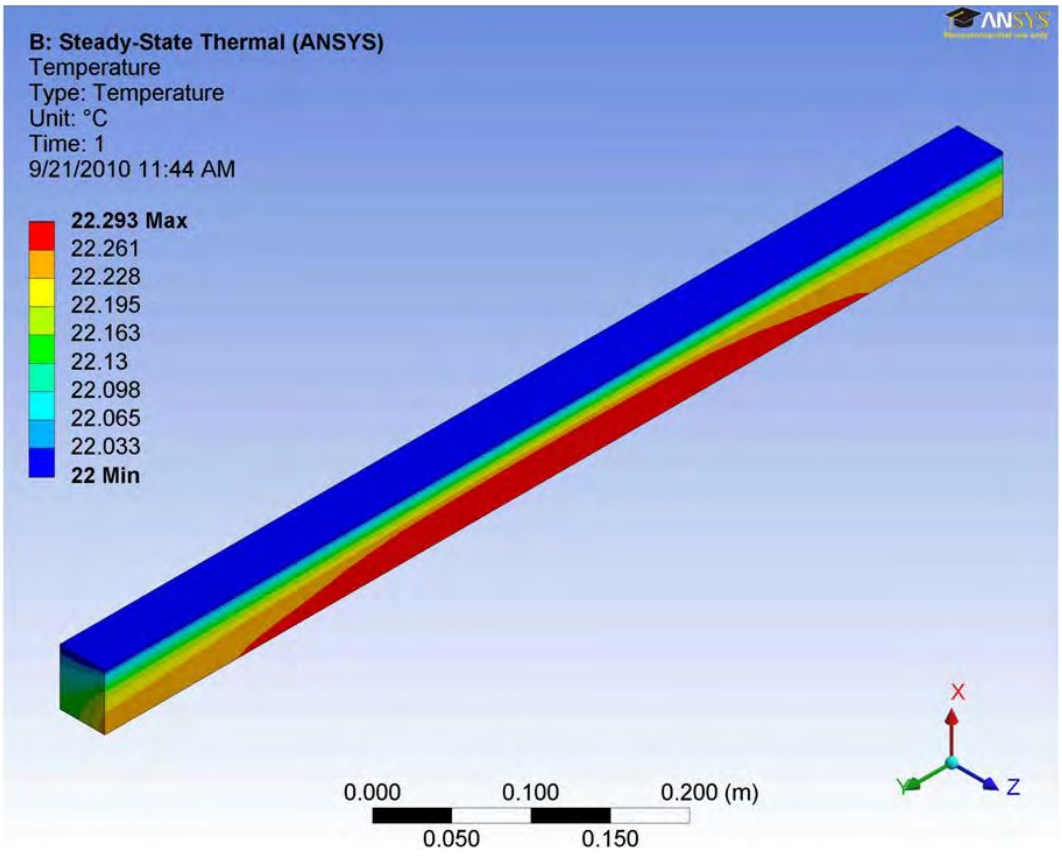


**Figure 13 - Showing typical temperature distribution with cooling on top only and no backlighting. Distribution remains the same when a film is added.**

The result of this first simulation with a single cooling surface is that the mirror bends outwards, opposite to the direction that we want it to bend, and downwards. The radius of the outward bending is 152 km, which is within one order of magnitude of the 20 km inward bending that we hope to achieve. This suggests that a backlight with double the power of the FEL beam and spontaneous radiation will still be well short of the design goal, giving a ~150 km inward bending, so at that stage the initial guess for backlight power to intentionally bend the mirror will be four times beam power.

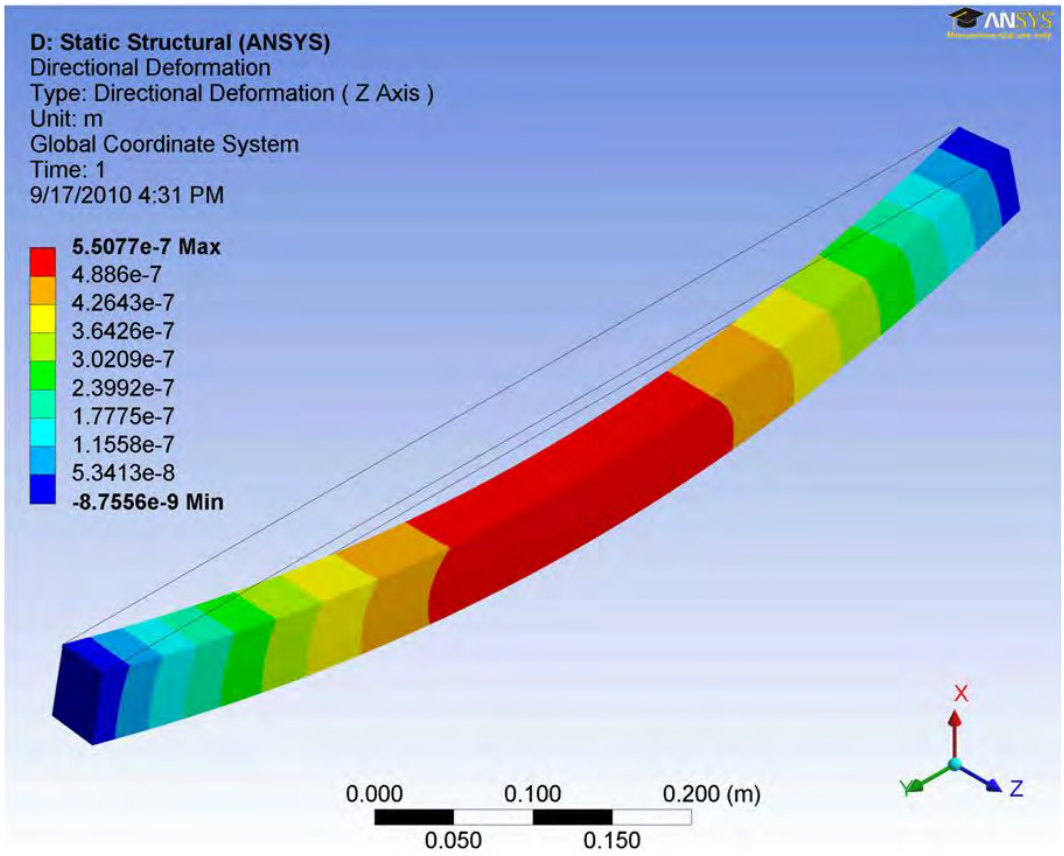


**Figure 14 – Z-deflection of weightless mirror with one cooled surface on top. The deflected shape bends in z and x.**

When only one cooling surface is used, on the top, and no heat comes in except for the X-ray load, the hottest spot on the mirror is on the front face near the bottom, which is not cooled. This spot is 0.29 °C hotter than the rest of the mirror.

***Liquid metal cooling on a single surface with heat lamp***

Since the first simulation confirms that the energy absorbed from the beam will create undesired bending in the mirror, the first idea that this paper will explore and simulate is to use extra heat, coming from the other side, to make the temperature distribution more homogenous; hopefully the mirror will remain straight in this case. In the interest of not touching the mirror, the heat would come from a lamp (see Figure 15). One benefit of this idea is that a halogen lamp is on the low end in terms of costs when talking about X-ray optics. While a heat lamp can come with a variety focusing mirrors of its own, we will idealize the effect of a heat lamp placed near the back side of the mirror as a homogenous heat flow to the back surface.

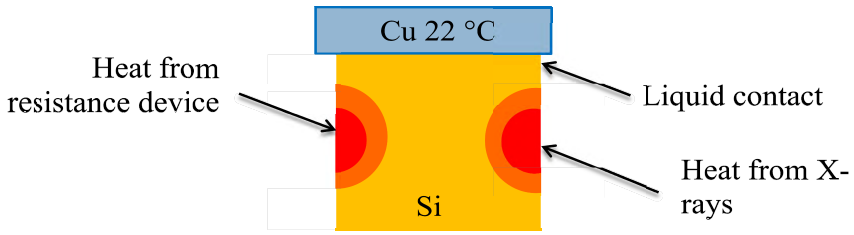


**Figure 15- Describing one cooled surface with added heat from a lamp. The cooled surface may also be on the bottom, and the mirror is assumed weightless.**

We expect the bending in this case to be up, towards the cooling plate, only. However, if the resistance input is 38 W to match the power of the absorbed X-rays on the other side, ANSYS shows that the mirror will also bulge towards the incoming radiation as it did before, only not as much. Why is this? While the heat lamp input is

diffuse, the FEL radiation is not. Since it has a peak intensity centered along the mirror length, it has an greater effect on bending than the more homogenous heating due to the *S* term. It turns out that bending in the z-plane is minimized when the diffuse heat lamp is set to $S\int dA + 1.7*\iint H(x,y)dxdy$; in other words, the FEL radiation has almost twice the impact on bending as the spontaneous radiation. So in Figures 16 and 17, the heat lamp was set to 43 W. This relationship was found by trial-and-error.

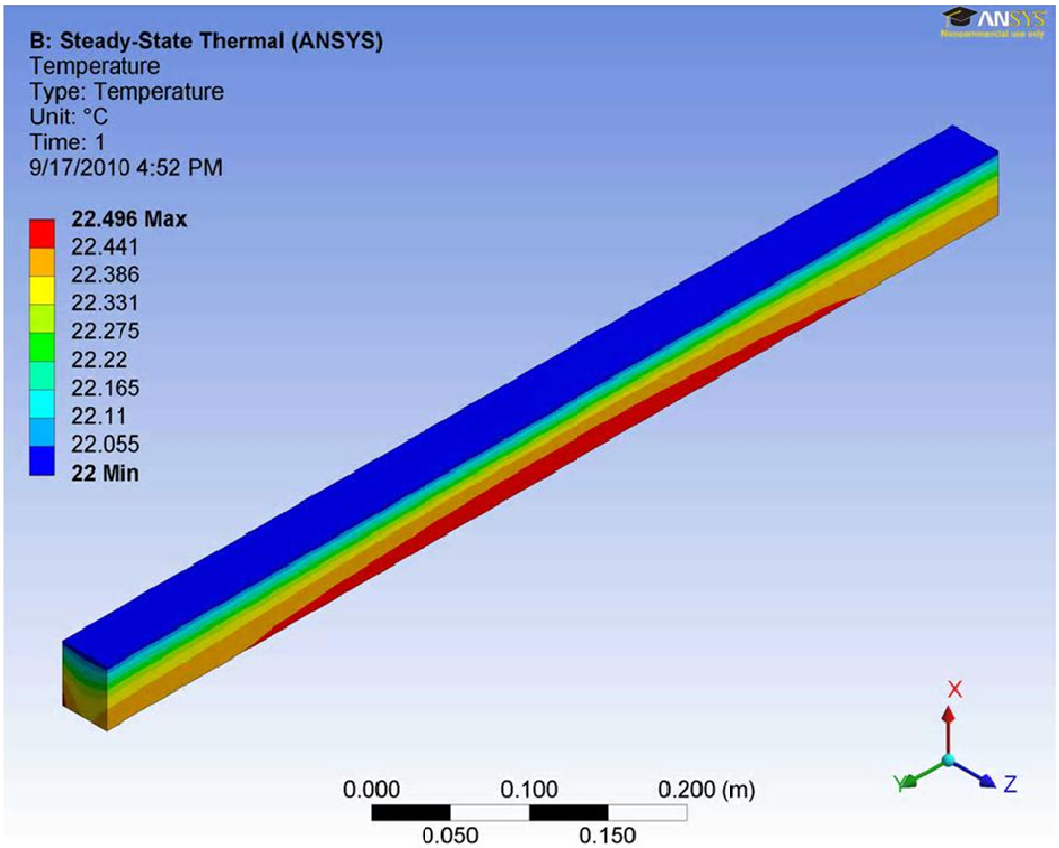


**Figure 16 – Temperature distribution with 43 W backside heat, one cooling surface. Max temperature is +0.5°C in this configuration.**

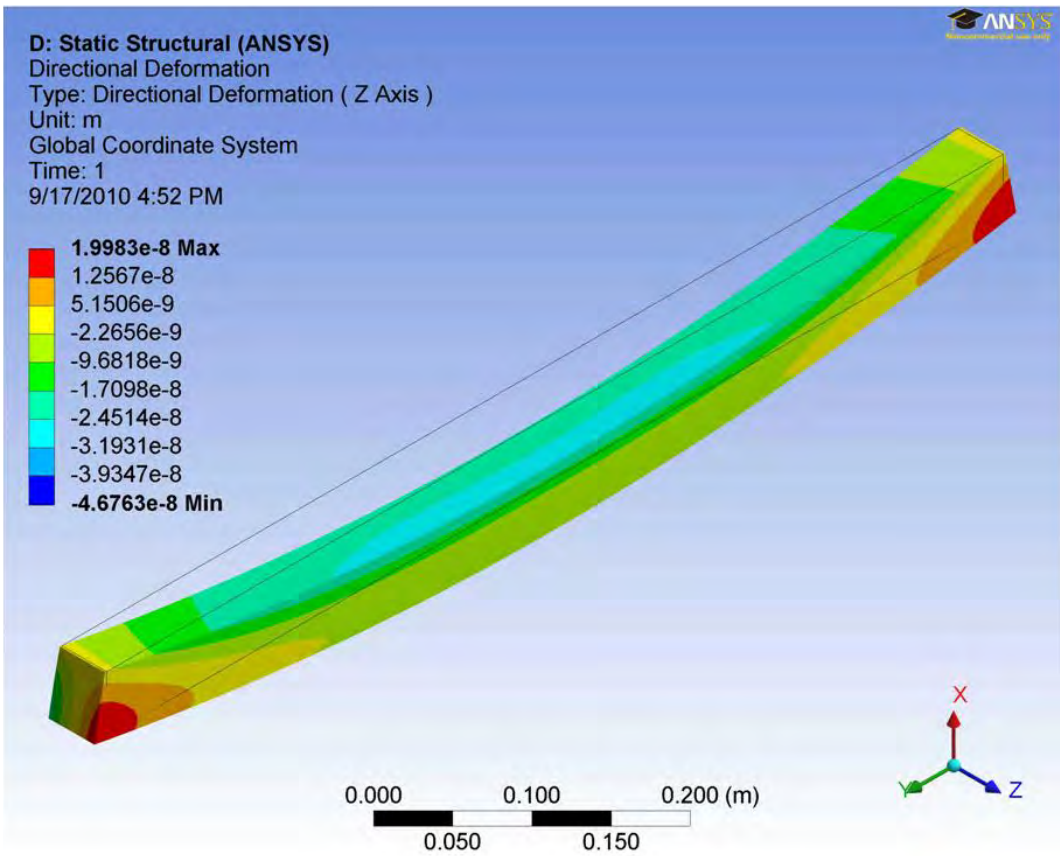


**Figure 17 – Z-deflection of mirror with one cooling surface and 43 W heat on back surface. This is the straightest configuration acheivable while in service using only a heat lamp, no second cooling surface or metal film.**

Even with this fine tuning, the z-deformation of mirror's front face has an increasingly strong gradient towards the ends, shown in Figure 17. Rather than being perfectly flat, the deformed shape in this case is best modelled by an inward circle of 2600 km radius, which should be near enough to infinity or flat for European XFEL's purposes. If the heat lamp used in practice is not diffuse relative to the back surface of the mirror, this relationship will change and the best approach again will be trial and error with the actual lamp. The deviation from the large circle, shown in Figure 18, is like a cosine wave with an amplitude of 4 nm. Our goal is to reduce this amplitude to 2 nm or

below. The plot is noisy because the large (>$10^6$ m) radius compared to the small error pattern (~$10^{-9}$ m) pushes the graphing software to the limit of its precision.

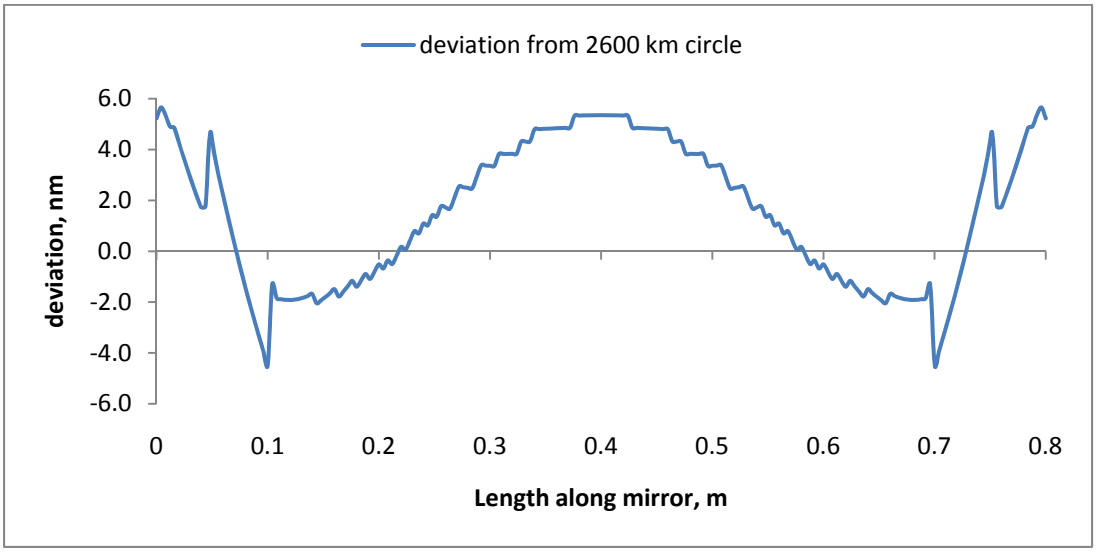


**Figure 18 – Bump created by FEL beam isolated from large-radius circular deflection. The large radius puts us at the limit of machine precision. Single cooled surface.**

The bending in the x direction (up) is not without consequence, however. As discussed before, there are anticlastic effects. In pure bending due to a single applied moment, the anticlastic bending would make the originally vertical planar face of the mirror slope slightly downwards. However, simulation shows that the average slope is actually 0.57 microradians upwards. Why is this? This is because isotropic thermal expansion plays a bigger role. The average temperature difference between top and bottom, looking back at Figure 16, is about 0.45 °C. Both the X-rays on the front and the heat lamp in the back cause this temperature difference. The thermal expansion of silicon is 2.6 μm/(m*°C), meaning that the expected slope from this effect in isolation is 0.29*2.6 = 0.75 microrad upwards. So the simulated average slope is equal to the effect of isotropic thermal expansion plus the unknown effect of anticlastic bending. The

magnitude of anticlastic bending is therefore about 0.6 microrad, constant along the mirror length.

The average vertical slope of 0.57 microrad is not a big deal; over the ~750 m remaining beam line, it amounts to a vertical beam displacement of 0.4 mm. This will not cause the beam to hit any barriers and is easily accommodated at the experiment site. What may be a greater concern is the variation in the vertical slope against this average, shown in Figure 19. We know that such variation is due to the uneven, Gaussian heat load only, not due to warping, so finding it at this stage will help us isolate the warping effect later.

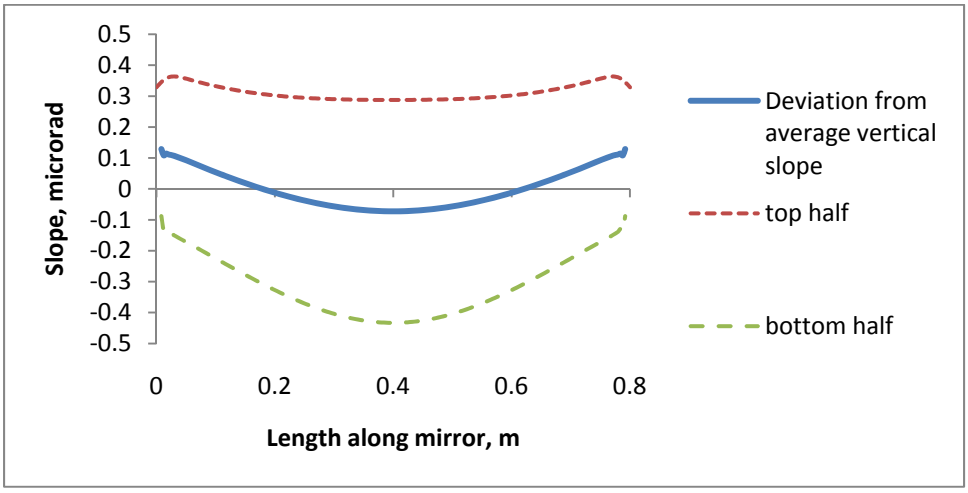


**Figure 19 – Variation in vertical slope of the front face due to uneven heating. Single cooled surface.**

***Cooling on a second surface***

There are a couple of ways to achieve cooling on the second surface. The mirror could be 'sandwiched' between two cooled copper plates, with a liquid metal interface on both sides. There could possibly be small channels cut in the top surface of the mirror as

discussed previously. For cooling on the bottom surface, the mirror could actually float in liquid metal instead of resting on a cooled plate. This also was discussed previously.

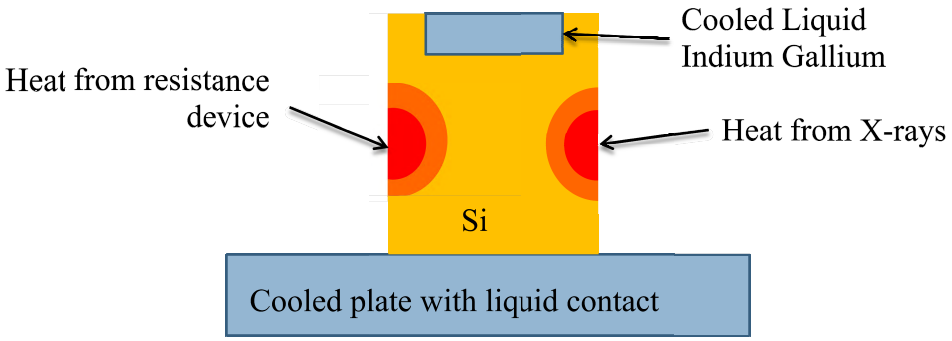


**Figure 20 – Showing one possible configuration to achieve cooling on top and bottom of mirror.**

If channels are used on top, the overall height of the mirror will be greater but the distance from the bottom of the channel to the bottom of the mirror would be the original 5 cm height. We can assume that a horizontal plane intersecting the bottom of these channels defines an isothermal surface nearly enough. Similarly, if the mirror is floating in a pool of liquid metal, some of the mirror would be submerged and therefore unusable. The mirror would first be designed so that 5 cm would still be above the 'waterline' and the same assumption could be made about a constant-temperature horizontal plane which would otherwise be the bottom of the mirror. For these reasons, the choice of how to cool is not especially important at this stage; it is more important to understand if there is a benefit in the first place before going much further.

The results of ANSYS simulation show that with symmetric cooling, the tendency to bend in the x-direction is eliminated, along with its attendant anticlastic effects in the

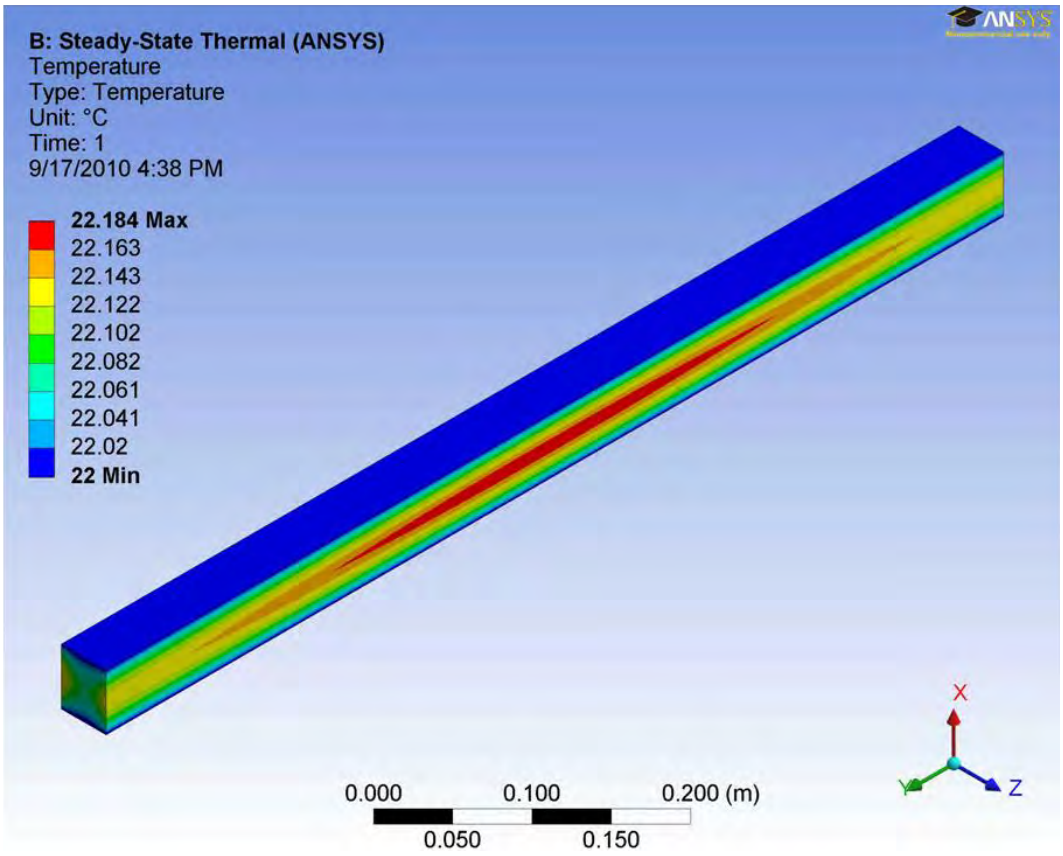


**Figure 21 - Temperature distribution with two cooling surfaces and 43 W backlighting. Max temperature is +0.18 °C. Back surface has wide band of higher temperature like front surface, without the ellipse in the middle.**

z-direction. However, there is still some bending in the z-direction. As before, the flattest shape possible corresponds to a backlighting input of 43 W, and the mirror seems to 'snake' in the z-direction. One bulge is visible for the front side view of Figure 22, and on the back there are two more.

However, these 'bulges' represent deflections that are very small, less than three nanometers in amplitude, shown in Figure 23. While this is an improvement over the 4 nm seen in the simulation with one cooling surface, the tolerable error according to Yamauchi et al was 2 nm. Because there are only three of them, the slope error is much less than the threshold of 3 microradians they also proposed.

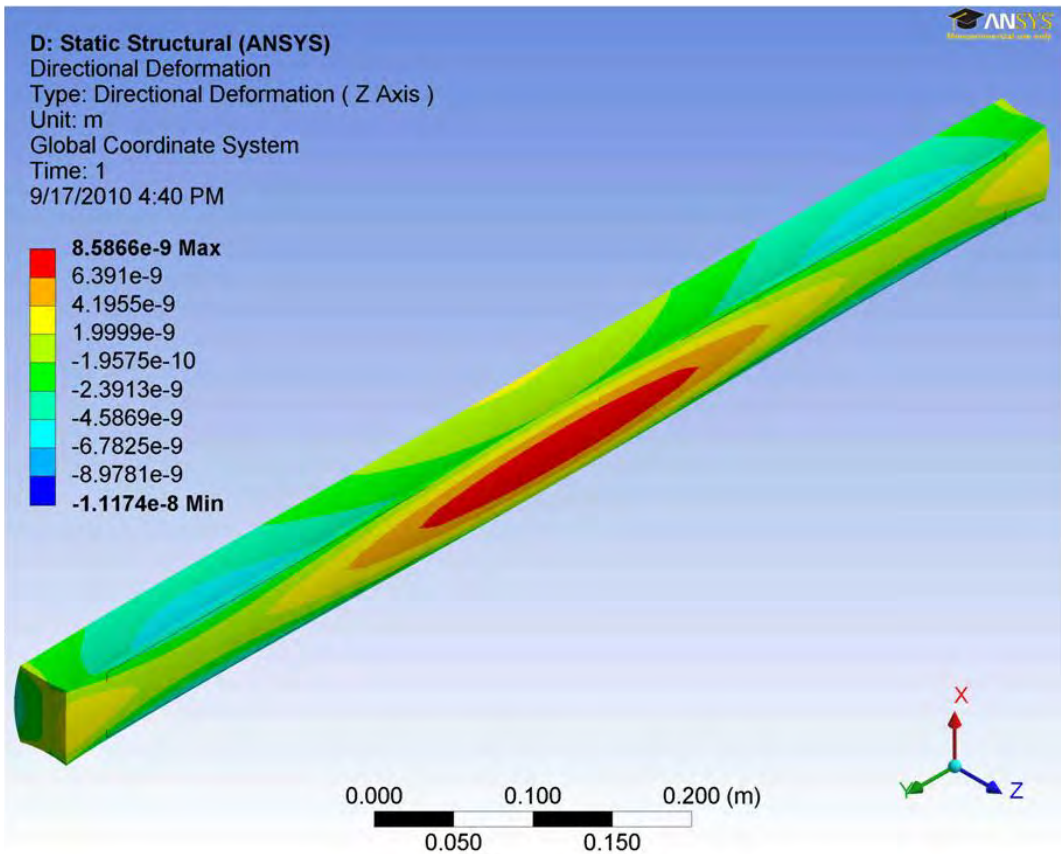


**Figure 22 – Z-deflection with 43 W backlight and two cooling surfaces. Main feature is central bump with amplitude of 3 nm.**

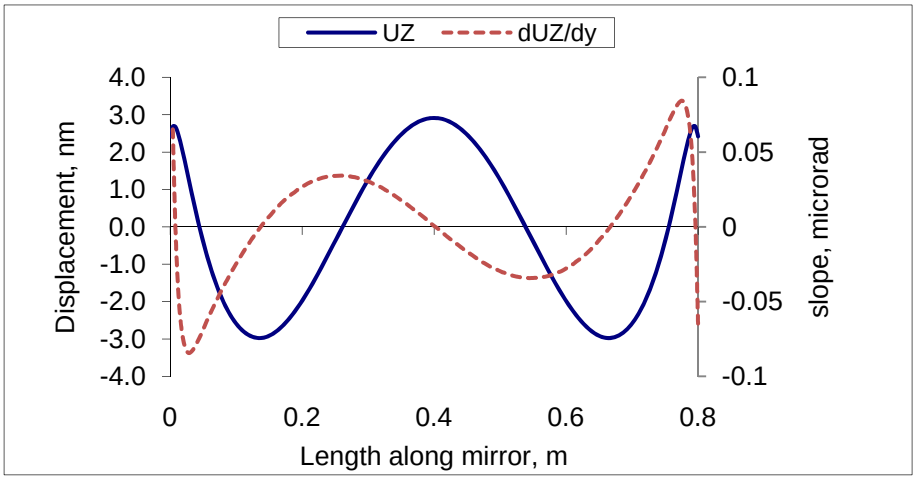


**Figure 23 – Deflection in Z direction along center line of mirror face. Attempting to keep the mirror flat.**

In the previous case with a single cooler we closely examined the vertical slope of the mirror, but in this case, as should be expected, the deflection profile along the top is identical to that along the bottom; both are the same shape seen in Figure 23 but with smaller amplitude. The vertical slope along the center is zero for the entire length.

*Increasing lamp power to bend mirror*

So far we have only considered how to keep the mirror flat, not how to use extra heat to bend it with a 20 km radius. Next, simulations were also run where, with two cooled surfaces, the power of the heat lamp is increased beyond optimal to create a surface that may not only reflect the beam but also focus it.

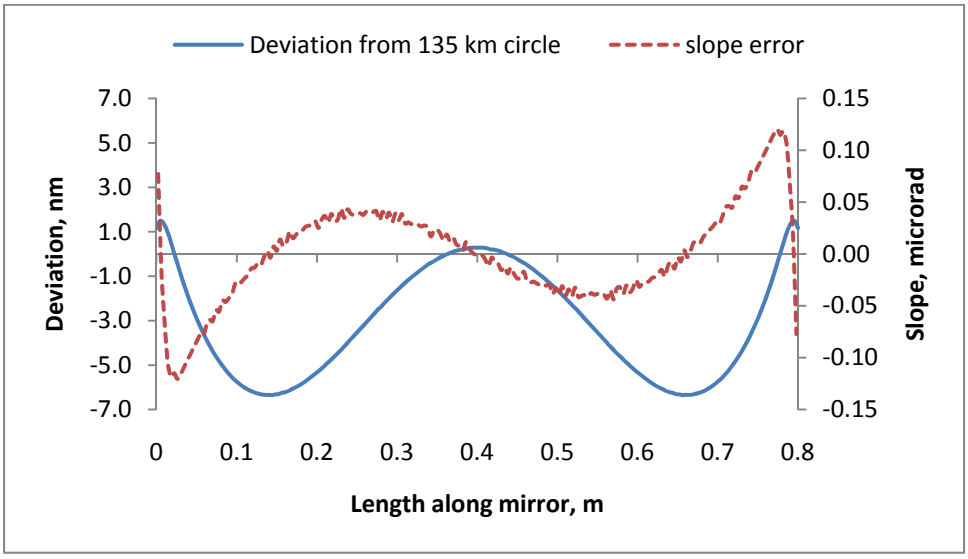


**Figure 24 – Results of using backlight @ 172 W to bend mirror. Amplitude of deviation increases beyond 4 nm. Two cooled surfaces.**

It turns out that, whether one cooling surface or two is used, extra heat does not seem to be the most profitable way to bend the mirror. With 172 W, that's four times the backlighting required to keep the mirror straight, simulation predicts the mirror bending radius as 135 km, still an order of magnitude away from the desired 20 km. The

deviation from true circular deflection due to the concentrated heat of the XFEL beam is slightly greater than it was in the previous case, where flatness was the goal.

It seems that using a heat lamp to bend the mirror is not a viable way because as the heat lamp requirement becomes greater, the load on the cooling system also increases. Removing a few hundred watts from a surface of this size is doable; the problem is more doing so in a way that creates a uniform temperature across the top and bottom. At greater heat loads the cooling fluid going through the copper plate or stainless bathtub will be appreciably hotter at near the outlet than near the inlet, creating another temperature gradient whose effect on bending must be considered. For this reason we conclude here that a heat lamp alone may be a viable option to keep a flat mirror flat, or a mirror machined with a curved surface curved, but it is probably not a good way to actively change the focus length of the mirror.

***Adding a metal film***

While the heat lamp keeps the mirror flatter than it would be with no intervention at all, a greater level of flatness and bending control is desired. To actively change the bending radius and therefore the focus length of the mirror, while minimizing the appearance of 'heat bumps', one final solution will be considered which is a metallic film. The film would be deposited by a CVD process at a certain temperature, and when used at temperatures other than the deposit temperature it will tend to form a curved shape, as discussed previously. Simulating the metal film is straightforward. The computer is told the bulk properties of the film and its thickness. A starting value 100 microns thickness was chosen after running some numbers through Stoney's equation. ANSYS has a variety of ways that it can model adhesion; we have chosen perfect

adhesion and we will monitor the shear stress to make sure this is always an appropriate choice. Another thing the ANSYS user must consider is the thermal interface between the film and the substrate. We chose the default setting which averages the two values of thermal conductivity for heat flow across the boundary. ANSYS will allow the user to program a unique value of interfacial conductivity in case there are small multilayer structures designed to insulate or conduct. A metal silicide layer, if allowed to form, would be a case like this. This will not be simulated here.

*20 km bending with 100 micron tungsten film and one cooling surface*

For the first iteration of this design, tungsten was chosen for the film material. The incoming X-ray heat load was kept the same, the initial temperature set to 22 °C, and the temperature of the top 'cooling' surface set to 58 °C, as if the temperature of the cooling water was allowed to change by 36 °C. The final temperature was selected by examination of Stoney's Equation (Equation 1). With these parameters, Stoney's Equation predicts a bending radius of 20 km as specified by Workgroup 73.

The temperature distribution in this case is identical to that shown in Figure 13, which also had one cooling surface and no backlight. The difference of course is that now the coldest point is 58 °C. This means that the film does not affect heat conduction. The deformation diagram is completely different however; the heat bump does not even show up in the display. Instead, the deformation at each node must be compared to the nearest circular shape to isolate the effect of uneven heating from the effect of thermal mismatch and also to find if warping is taking place.

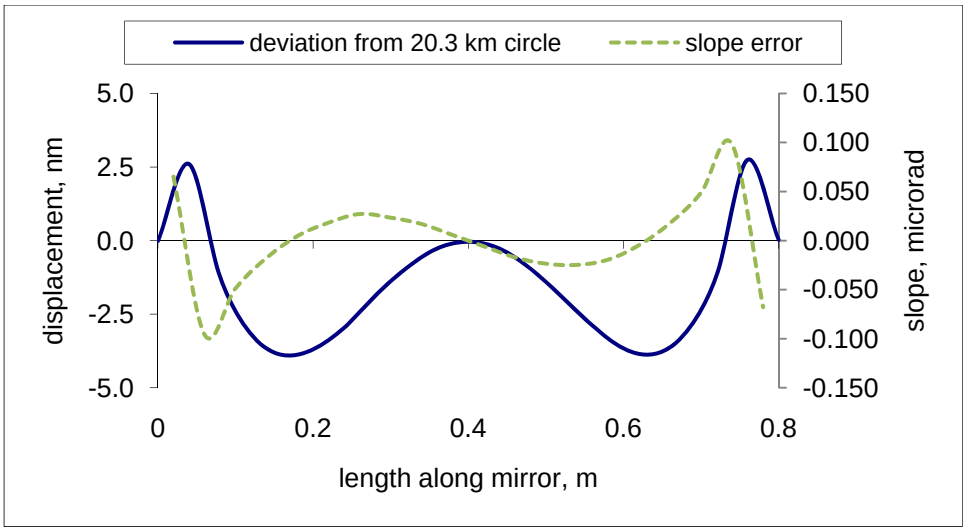


**Figure 25- 20.3 km circle subtracted from deformation in z-direction.**

**Tungsten, $t_f$= 100 µm, ΔT=36 °C, top cooling only**

Figure 25 shows that the shape of the deviation from circular profile is similar to the previous deviation from flat in Figure 24. There is a central bump in a sinusoidal pattern whose amplitude is about 3.5 nm. This suggests that the effect of the film and the effect of the uneven heating have little interaction; the principle of superposition seems to work here though not perfectly so.

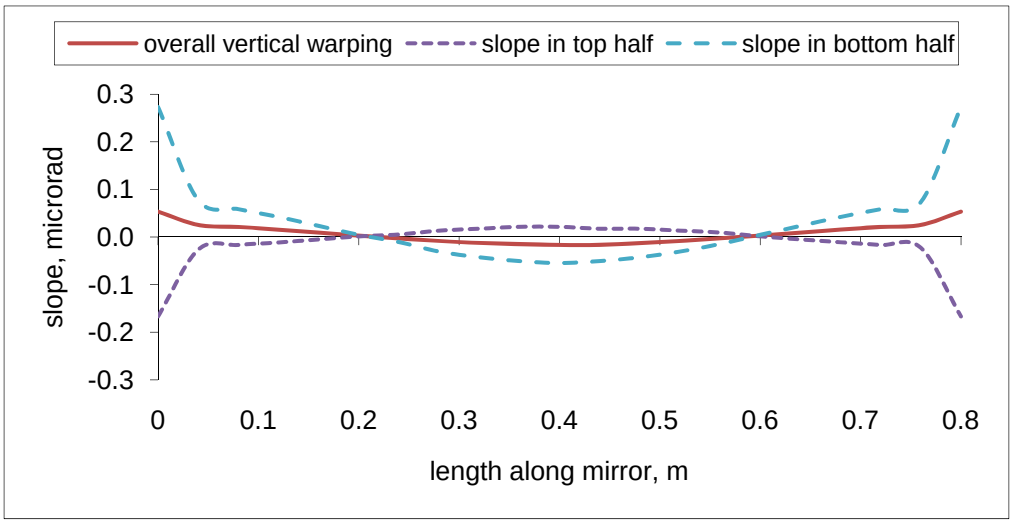


**Figure 26- Vertical Slope dx/dy. Tungsten, $t_f$= 100 µm, ΔT=36 °C, top cooling only**

Figure 26 shows that the slopes in the vertical plane have the same inclination as they did in the prior 'no film single cooler' simulation of Figure 19. The magnitude is much smaller, however. This suggests that warping due to stiffness mismatch in fact plays very little role. Instead the increased stiffness seems to greatly reduce the effect that uneven heating has on the vertical slope, even slightly reducing the amplitude of deviation from 4 nm (Figure 18) to 3.5 nm in Figure 25.

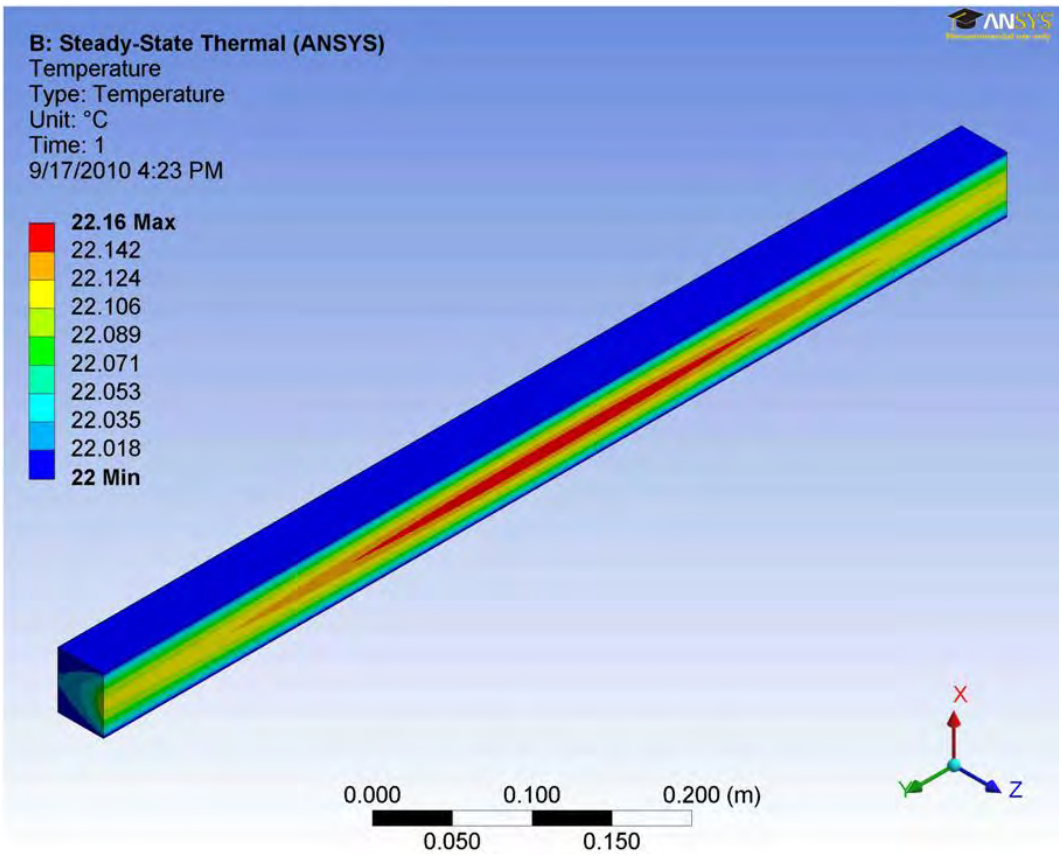


**Figure 27 – Temperature distribution with two cooling surfaces and no backlighting. The distribution remains the same when a film is added. Max temp is +0.16 °C. Back surface has near constant temperature.**

*20 km bending with 100 micron tungsten film and two cooled surfaces*

The next simulation is the same as the previous one, except that this time both the top and bottom are cooled. The nearest circular shape, in this case, has a radius of 19.5 km, very close to the previous value of 20.3 km and both are sufficiently close to the design value of 20 km. The reason for the variance from the 20 km spec is the Gaussian heat generation function in the simulation. We would expect that the uneven heating would create a deviation from the circular shape roughly the same size as the deviation seen in each previous simulation. However, this is not the case. The second cooled surface and removal of the backlight together reduce the overall anomaly in the temperature distribution. With two cooled surfaces, the deviation from circular with a tungsten film is down to an amplitude of 2 nm, compared to 3.5 nm with a film and one cooled surface and 3 nm with no film and a 43 W backlight.

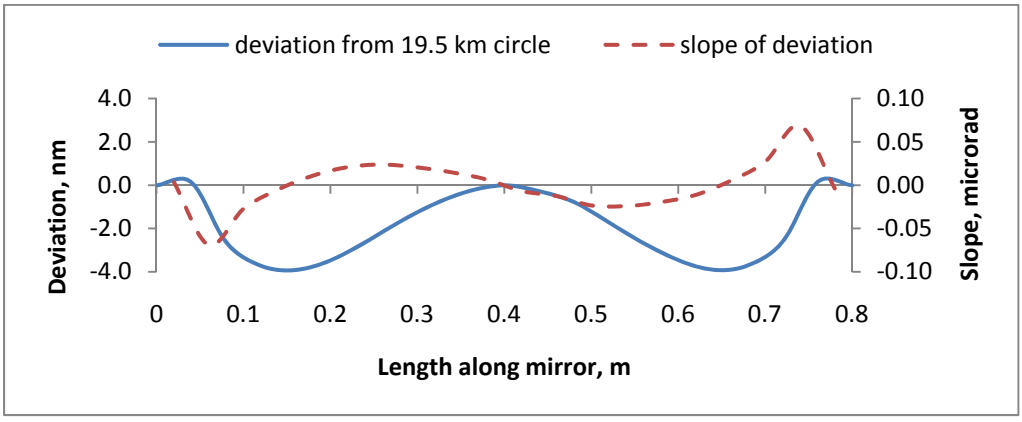


**Figure 28 – Using a 100 micron Tungsten film with a 36 °C temperature change to induce bending, graph shows deviation from circle due to FEL radiation. Amplitude of deviation less than 2 nm.**

If the vertical slopes examined previously were a concern, using two coolers eliminates them to a great extent. This is shown in figure 29. Since the temperature gradient shares a plane of symmetry with the undeformed mirror and film, the vertical

slope in the top half is a mirror image of the vertical slope in the bottom half and the sum is zero. The magnitudes are also very small, the 0.25 microrad maximum is found at the edges only. It was feared that significant vertical slopes might appear as the film created warping. This did not occur; the fear about warping seems to be unfounded.

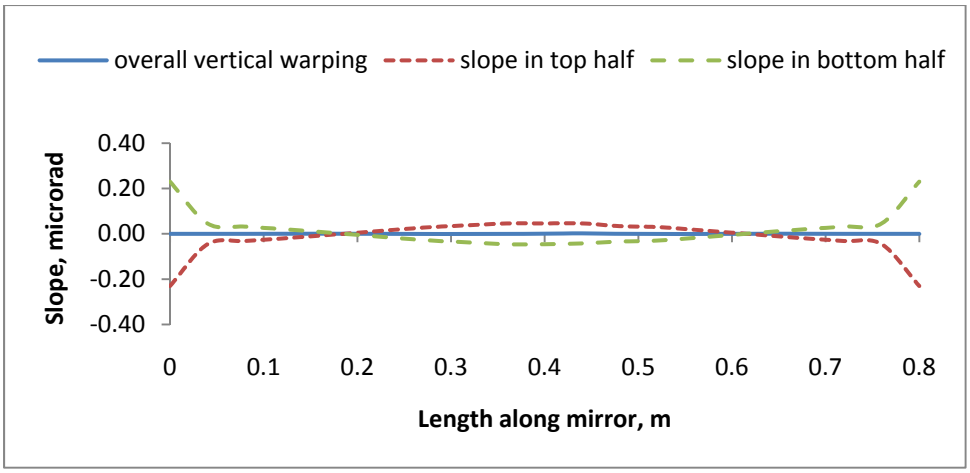


**Figure 29 – Vertical slopes along mirror with tungsten film. $t_f$= 100 µm, ΔT=36 °C, cooling on top and bottom**

*Considering other materials*

After examining this first set of results, one concern is that the 36 °C temperature difference requirement is too steep; it may be difficult to find a water delivery system with that kind of range as well as precision. Plus, the greater the temperature difference between the flat 'infinite radius' state and the 20 km minimum radius, the more prohibitive changing the mirror state will be for researchers, in terms of time required to set up an experiment. One course of action would be to increase the thickness of the tungsten film, but this requires more time and money to fabricate. The obvious step is then to examine other materials with greater thermal mismatch and differing stiffness. Almost every metal has a greater expansion coefficient (α) than silicon, but as it turns

out, tungsten's is among the lowest of the metals. Metals have a wide range of stiffness values, (E). Table 1 compares tungsten to other candidate metals and Figure 31 graphically shows the selection process.

**Table 2- Relevant properties of materials discussed here**

| Pure Material | E (GPa) | α ($\mu K^{-1}$) | Deposit Method | Notes |
|---|---|---|---|---|
| Silicon | 185 | 2.6 | N/A | |
| Tungsten | 400 | 4.5 | CVD | Excellent adhesion |
| Nickel | 200 | 13.4 | CVD | Good adhesion, no reaction below 300°C |
| Copper | 110-128 | 16.5 | PVD | More reactive to silicon than others |
| Beryllium | 287 | 11.3 | ? | Toxic, Reactive in air, may need protective Ni coating electroplated after deposit |

Nickel and copper immediately stand out as perhaps better choices, if maintaining film thickness near 100 μm is the goal. Both, however, have lower stiffness than tungsten. At this point it is believed that the greater stiffness of the tungsten reduced the size of the bump created by the concentrated FEL beam. Stoney's Equation suggests that if nickel is used instead of tungsten, only a 12 °C change is necessary for a 100 μm film to induce a 20 km bent radius, however nickel's lower stiffness may give inferior results.

*20 km bending with 100 micron nickel film and two cooling surfaces*

So the previous simulation with two cooled surfaces and a metal film was changed from tungsten to nickel, and ΔT was changed from 36 °C to 12 °C, and the simulation was re-run. Figure 30 shows that the deviation from flat or circular has an amplitude of 2.5 nm with a 100 micron nickel film, reducing as film stress increases. The

reduced stiffness of nickel does not seem to play a role in minimizing the deviation. Interestingly, the deviation also gets smaller as the mirror bends more due to film action.

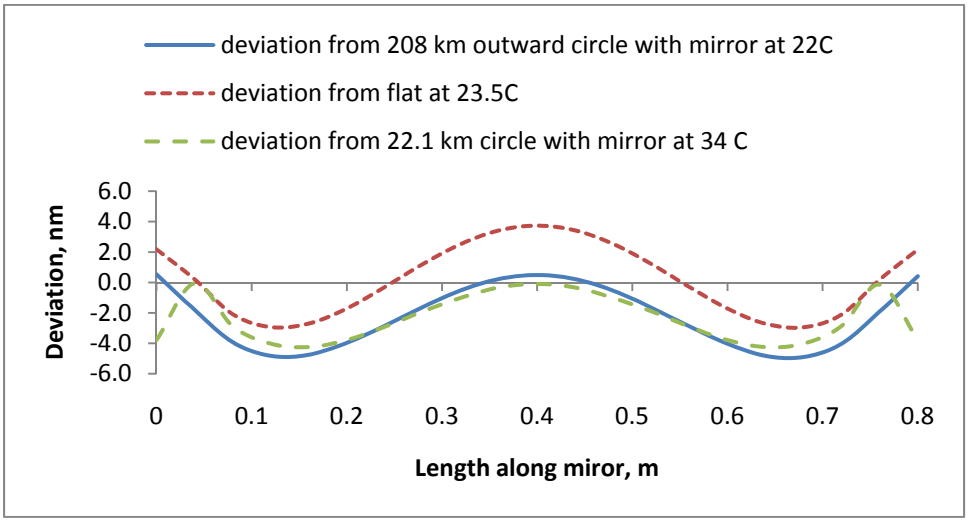


**Figure 30 - The effect of a 100 µm Ni film, deposited at 22 °C, on mirror behavior**

*20 km bending with 300 micron tungsten film*

If film stiffness is the key to keeping the bent profile as circular as possible, minimizing deviation, taking the stiffest material under consideration and increasing the thickness seems like a good play. Stoney's Equation says that if a tungsten film is used at 300 microns, the temperature change needed to produce 20 km bending is 12 °C, which makes sense because increasing the film thickness by a factor of three should reduce the temperature change by the same factor, everything else being constant. However, simulation predicts that increasing the film thickness with tungsten actually makes matters worse. When the film was 100 microns tungsten, with two cooling surfaces, the deviation from the nearest circle was 2 nm in amplitude. With increased tungsten thickness it is back up to three. The only intrinsic part of the system that changed when film thickness was increased was the film stress. This suggests that high film stress, and not the thickness of the film alone or its stiffness alone, is what acts to minimize the FEL

bump size. The recommendation that will follow, then, will likely bring the film stress near to the edge of the tensile or delamination level, whichever is less.

Looking at Figure 31, we can now make an informed decision about the best film material. Stoney's equation, as previously derived for the film shear stress, is complicated but it can be shown that the stress will increase linearly with the film's expansion coefficient. However, when there is a fixed goal for a bending radius, the only result of increasing the expansion coefficient is reducing the needed temperature change. The shear stress is a function of the film thickness, but not the stiffness or thermal expansion of the film, when the radius of curvature is fixed. There are stiffness terms, Young's Modulus E and Poisson's Ratio nu, but they belong to the substrate.

$$\tau_f = \frac{E_s \cdot (t_s)^2}{6 t_f \cdot (1 - \nu_s) r} \cdot \left(1 + \frac{4 t_f}{t_s}\right)$$

**Equation 9 – Stoney's Equation solved for film stress with a known radius of bending. The equation becomes simpler when the radius of curvature, r, is known.**

Thus the decision of which material to use is not driven by a desire to minimize the deviation due to concentrated heating. Instead it is driven by the power of the cooling system, that is, what magnitude of change in temperature it is capable of over a short period of time. It is also driven by the adhesion strength and yield strength of the material. While a nickel film will achieve desired performance with a smaller change in temperature, there is less documentation available about the adhesion strength of such films, compared to tungsten. For both films, it is presumed that the adhesion strength is the controlling factor; that is that some type of delamination is likely to occur before the film material yields intrinsically.

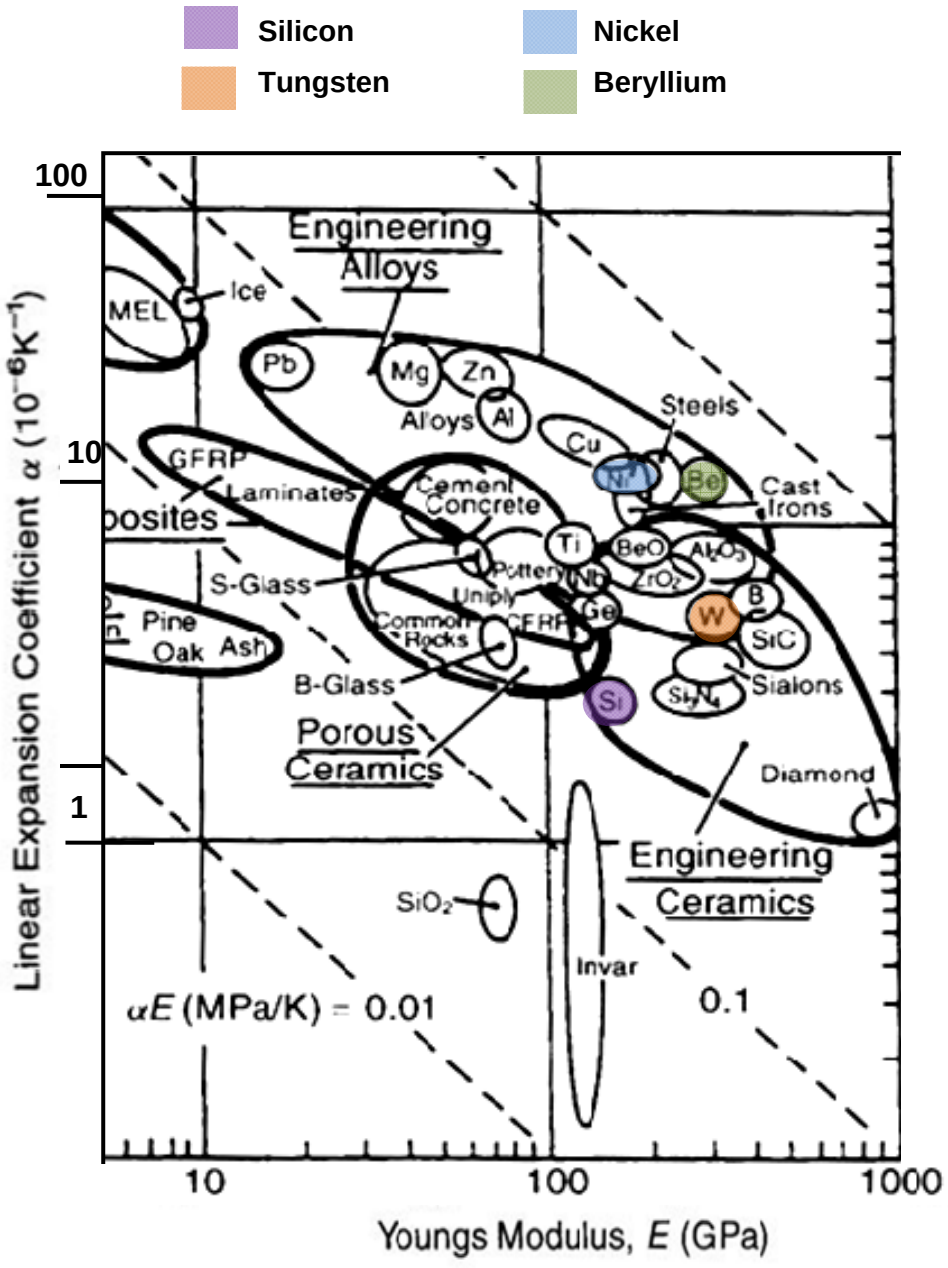


**Figure 31 – Adapted from Ashby Material Selection Charts, used with permission[20]. The ideal film material, in addition to good adhesion to silicon and low reactivity, has an elasiticity similar to Silicon with a large coefficient of Thermal Expansion.**

*Keeping the mirror flat with a metal film*

As discussed previously, the XFEL beam alone is already bending the mirror the wrong way before we start to talk about heat lamps and metal films to bend it the right way. No matter what metal film is used, or what the thickness, if the mirror begins to handle X-rays while the cooling system is set to the film deposit temperature, the mirror will bend the wrong way. The magnitude of this bending is reduced by the effect of the film stiffness, but the direction is not changed.

For this reason simulations were run for the purpose of knowing what change in temperature gives the flattest mirror for each film configuration.

**Table 3 – Temperature change that will keep the mirror flattest in presence of concentrated FEL heating**

| Film material | Thickness | Flat temperature |
|---|---|---|
| Nickel | 100 µm | +1.5K |
| Tungsten | 300 µm | +1.1K |
| Tungsten | 100 µm | +4.6K |

***Buoyant cooling bath***

A buoyant support has an obvious advantage and an obvious disadvantage. The advantage is that we know that a dense liquid will support the mirror homogenously, without any risk of creating extra stresses. The disadvantage is that a fraction of the mirror would be submerged, and the mirror may tilt in this arrangement. The liquid proposed, as stated before, is Indalloy 51, which has a specific gravity of 6.5. The silicon that would float in this liquid has a specific gravity of 2.33, or 35% of the density of the liquid Indalloy 51, therefore 35% of the silicon would be submerged. This means that to have a usable area of 5 cm, the original manufactured mirror height must be 6.7 cm.

A second, related problem to a buoyant support appears if a metal film is used. The solid metal film will be denser than its silicon substrate, unless the film is beryllium which is slightly less dense. This difference in density will mean that the center of mass is away from the center of volume. These two centers must be vertically aligned for the mirror's floating orientation to be vertical, meaning if nothing were done the mirror would tilt backwards as it floats, the side with the film sinking and the optical side rising. This problem could be solved with something as simple as a well-placed blob of dense putty, or perhaps the optical surface could be machined at the exact tilt needed to counteract this effect. Either way, the tendency of the mirror to tilt backwards must be considered if both a mirror with a film is used with a buoyant support.

## Ch. 4 Recommendations

***Response time considerations***

It is not enough for the mirror to merely exist and hold a certain shape at two different temperatures. We would like to know that it doesn't take 48 hours, or even an hour, for the mirror configuration to change. While the second cooling surface turned out to have less than the expected impact in minimizing displacement along the mirror face, obviously having double the cooling area will have a large impact on the amount of heat stored in the mirror and how much time is required to dissipate it and change the mirror configuration.

In none of the previous simulations were bumps due to the XFEL beam eliminated. Obviously, however, once the beam is turned off, they go away, after a certain period of time. Once the mirror is perfectly flat again, it takes the same amount of time for the steady-state deflection patterns previously discussed to reappear after the beam is turned on.

The consequence of the transition time between 'beam off' and 'beam on' is that experiments carried out within the transition time will be exposed to a slightly different beam than those that wait until steady state. If there is an important difference between the two, the experimenter will have to keep the final set of shutters closed during one phase or the other.

So, it will be helpful to make a small introduction to transient thermal problems, apart from just simulating them. Fourier's law of heat transfer states that the rate of change in temperature of any point is proportional to the sum of all thermal gradients at that point. This gives the differential equation which applies uniquely at each point in space.

$$\partial T/\partial t = \alpha[\nabla T]$$

**Equation 10 - Simplified Fourier Heat Equation**

α is the heat diffusivity of the material. This typical first-order partial differential equation has solutions for *T(x,y,z,t)* that are dependent on the initial and boundary conditions but always include a term $e^{-\alpha t}$ for exponential decay. This is typically the only term that involves time, unless one of the boundary conditions also varies with time. So, when the question is asked, "How long does it take to go from the initial state to the final state," formally, the answer is "Forever." The value of an exponential decay function approaches a final value as a limit but theoretically always comes up short. This leaves us dealing with terms such as "half life" which means, "the time after which the system is halfway between its initial and final states." To describe the time required for the mirror to reach a certain steady state, it seems best to think about "99% time" meaning "the time at which the initial difference between the maximum and minimum temperature of the mirror has reduced to 1% of its original value." This time depends on the material properties and dimensions and alignment of boundary conditions only, and has nothing to do with the initial or final state. For a silicon mirror cooled on the top only, the 99% time is 65 seconds. For a mirror cooled on the top and bottom, the 99% time is only one-quarter of that value. This is because there is twice as much surface area through which

heat can leave, and the maximum length from any point in the mirror to a cooled boundary has decreased by half. These figures were taken from a brief simulation with no film. The thin metal film did not change these values significantly.

***Most effective design, conclusions***

The most effective design is one that minimizes deformation due to the FEL beam while having a good response time. This study has shown that while an extra heat lamp can reduce this deformation, using a metal film was more effective. The most effective metal film is one that creates the most thermal stress. Finite Elements simulation shows that thermal stress in the film on the back side minimizes thermal strain on the front side. The effect is probably analogous to what happens when a bolt is pre-tensioned. The following table lists each configuration that was considered in Chapter 3 and lists the thermal stress in the film as well as the amplitude of the deviation from circular shape in the mirror; they seem to be inversely proportional.

**Table 4 – Interventions to bend the mirror to a 20 km radius**

| Film material | Film Thickness | Temp change for r= 20 km | Shear stress | Amplitude of deviation | |
|---|---|---|---|---|---|
| | | | | Top cooling | Sym cooling |
| Tungsten | 100 μm | 33 K | 34.2 MPa | 3.5 nm | 2 nm |
| Tungsten | 300 μm | 11.5 K | 11.5 MPa | 3.8 nm | 3 nm |
| Nickel | 100 μm | 11 K | 34.2 MPa | -- | 2nm |
| No film, 172 W lamp power causing 135 km bending | | | | -- | 3.5 nm |

**Table 5 – Interventions to keep the front of the mirror flat.**

| Film material | Film Thickness | ΔT | Cooling | Shear stress | Amplitude of deviation |
|---|---|---|---|---|---|
| Tungsten | 100 μm | 4.5 K | Top only | 4.7 MPa | 2.5 nm |
| | | 3.3 K | Top and bottom | 3.4 MPa | 3.4 nm |
| Tungsten | 300 μm | 1.1 K | Top and bottom | 1.5 MPa | 5 nm |
| Nickel | 100 μm | 1.5 K | Top only | 4.7 MPa | 3.4 nm |
| No film, 43 W backlight | | -- | Top only | -- | ~4 nm |
| | | -- | Top and bottom | -- | 3 nm |

For the design process to continue from here, more information will be needed about the CVD process and the adhesion strength expected, and the cooling system and how quickly the temperature of the cooling water may be changed. Cooling both on the top and the bottom are recommended for the 75% shorter response time and the reduced deviation both from flat and from circular.

For film selection, the rule of thumb will be that thinner metal films working with larger temperature changes will produce the best results both in the flat state and in the curved state. A second rule of thumb is that for a given thickness of tungsten film on a 4 cm thick silicon mirror, the temperature change, in degrees Kelvin, required to create a 20 km bend is roughly equal to the shear stress generated, in MPa.

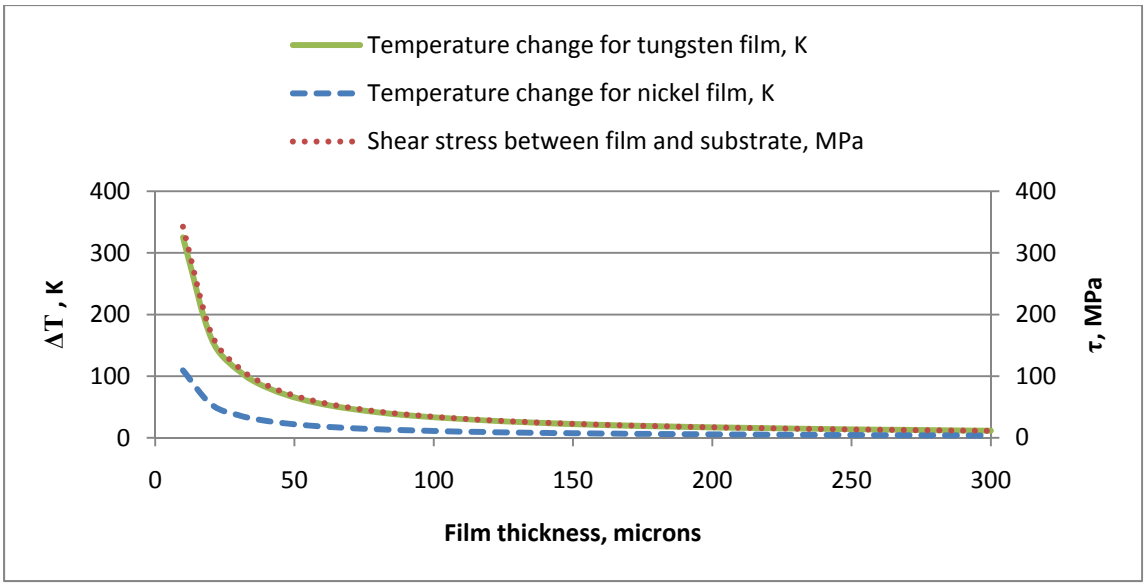


**Figure 32 – Guide for film selection using Stoney's Equation.**

***Future work***

Future work could go in two directions from this juncture. For those working at European XFEL, future work would center on practical considerations such as the water/coolant delivery system, whose characteristics will drive the desired film properties. Commercially available metal coating processes must also be investigated and compared to the ideal room-temperature CVD envisioned here; again the three requirements for the film metal are 1) able to be strongly and inexpensively deposited to silicon (maximizing film stress without failure), 2) minimally reactive to air and liquid metals, and 3) the higher the coefficient of thermal expansion, the better. If the deposit temperature selected is much warmer or colder than room temperature, the cooling system much account for this.

The second direction that future work could go in is to simulate multilayer systems that might more effectively create the kind of constraining stress documented here, over a more practical range of temperatures.

## References


[1] Original image and caption from Hawkins and Staff Hawkins Electrical Guide Number One (New York: Theo. Audel and Company, 1917) 133, reworked, Copyright: 2009, Florida Center for Instructional Technology.

[2] Proprietary claim made online, http://www.xfel.eu/overview/facts_and_figures/ Retrieved 10/4/2010

[3] Harald Sinn, "Heat load estimates for XFEL beamline optics." Internal XFEL development document.

[4] Cameron Kewish, et al, "The potential for two-dimensional crystallography of membrane proteins at future X-ray free-electron laser sources," New Journal of Physics, 12, 035005 (2010).

[5] Kazuto Yamuchi et al, "Wave-optical evaluation of interference fringes and wavefront phase in a hard-X-ray beam totally reflected by mirror optics," Applied Optics, 44, 32, 6927 (2005)

[6] Michael Sullivan, et al, "White –light X-ray focusing mirror," Rev. Sci Instrum. 79, 025101 (2008)

[7] Michael Hitchman, et al, "Some considerations of the thermodynamics and kinetics of the Chemical Vapor Deposition of Tungsten," Applied Surface Science, 38, 312 (1989)

[8] Marketing claim made by manufacturer online, http://www.cvmr.ca/nvd/process.html Retrieved 10/4/2010

[9] D.C. Meyer, T. Leisegang, A.A. Levin, P. Paufler, A.A. Volinsky, "Tensile Crack Patterns in Mo/Si Multilayers on Si Substrates Under High-temperature Bending," Appl. Phys. A 78, pp. 303-305, 2004

[10] George Vander Voort, Atlas of time-temperature digrams for nonferrous alloys, A S M International, 1991 p. 462

[11] K.N. Tu et al, Thin Films- Interdiffusion and Reactions, Interscience, New York, 1978, p. 359

[12] Sheng Yuan et al, "Elliptically Bent X-ray Mirrors with Active Temperature Stabilization," X-ray optics and Instrumentation, 2010 784732.

[13] W.D. Nix, "Mechanical Properties of Thin Films," Lecture notes prepared for Stanford University in 2005 and available online at http://imechanica.org/node/530. Retrieved 9/16/2010.

[14] Michael R. Sullivan et al, "Installation and testing of a focusing mirror at beamline X28C for high flux x-ray radiolysis of biological macromolecules," Rev. Sci. Instrum. 79, 025101 (2008)

[15] Jean-Jacques Fermé, "New Improvements in Bendable Mirrors," Proc. SPIE 3152 (1997)

[16] Marketing claim made by manufacturer online, http://seso.com/pub/Glidcop%20cooled%20mirror.ppt Retrieved 8/16/2010.

[17] Kazuto Yamuchi et al, "Wave-optical evaluation of interference fringes and wavefront phase in a hard-X-ray beam totally reflected by mirror optics," Applied Optics, 44, 32, 6927 (2005)

[18] Hidekazu Mimura et al, "Direct determination of the wave field of n X-ray nanobeam," Physical Review A, 77, 015812 (2008)

[19] See 16

[20] Lecture notes available online at http://mielsvr1.ecs.umass.edu/mie497a/Ashby%20Materials%20Selection%20Charts.PDF. Reprinted here with permission from Dr. Mike Ashby.

**Appendices**

***Appendix A- ANSYS Inputs***

This Appendix section shows the report generated by a typical run of ANSYS 12 Workbench. This particular case is with a 100 micron tungsten film, one cooling surface, and a 4.5 K temperature change meant to keep the mirror flat while the beam is on. All other cases will be similar. This report should answer any detailed question about how the model was set up.

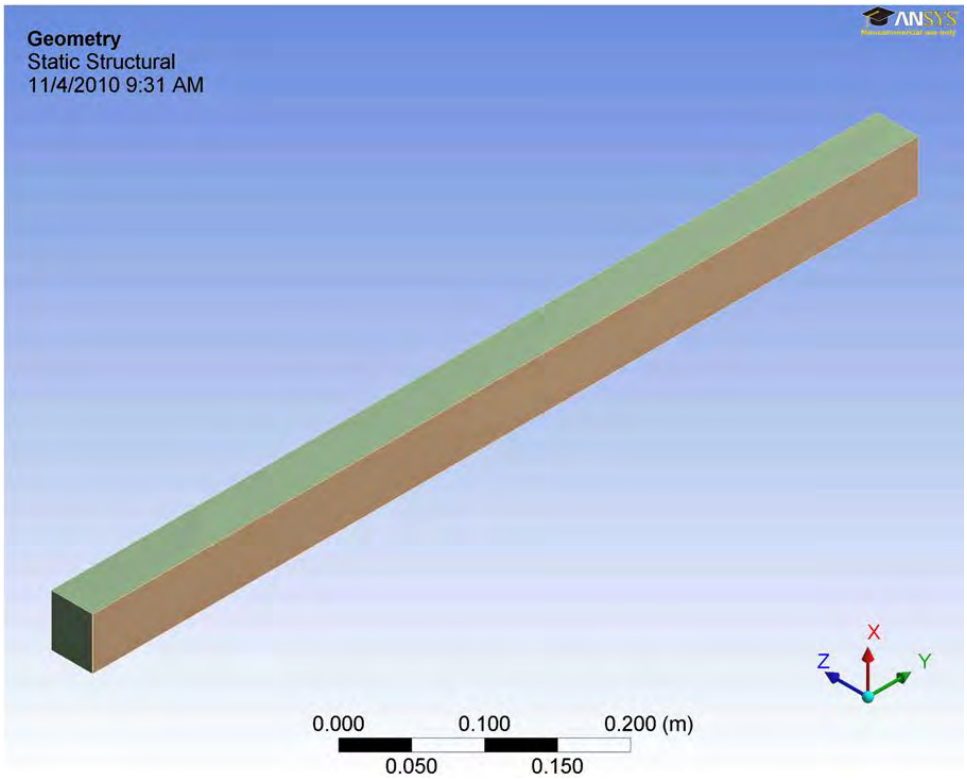


**Figure 33 - Simulated mirror, green, with thin film in orange.**

***Appendix A (Continued)***

*Units*

**Table 6 – Simulation units**

| | |
|---|---|
| Unit System | Metric (m, kg, N, s, V, A) Degrees rad/s Celsius |
| Angle | Degrees |
| Rotational Velocity | rad/s |
| Temperature | Celsius |

*Model (B4, C4, D4)*

*Geometry*

**Table 7 - Model (B4, C4, D4) > geometry**

| | |
|---|---|
| Object Name | *Geometry* |
| State | Fully Defined |
| **Definition** | |
| Source | E:\THESIS\Ansyssimulation\091710_files\dp0\Geom-1\DM\Geom-1.agdb |
| Type | DesignModeler |
| Length Unit | Millimeters |
| Element Control | Program Controlled |
| Display Style | Part Color |
| **Bounding Box** | |
| Length X | 5.e-002 m |
| Length Y | 0.8 m |
| Length Z | 4.01e-002 m |
| **Properties** | |
| Volume | 1.604e-003 m³ |
| Mass | 3.805 kg |
| Scale Factor Value | 1. |
| **Statistics** | |
| Bodies | 2 |
| Active Bodies | 2 |
| Nodes | 12027 |
| Elements | 2000 |
| Mesh Metric | None |
| **Preferences** | |
| Import Solid Bodies | Yes |
| Import Surface Bodies | Yes |
| Import Line Bodies | No |
| Parameter Processing | Yes |
| Personal Parameter Key | DS |
| CAD Attribute Transfer | No |
| Named Selection Processing | No |

*Appendix A (Continued)*

| | |
|---|---|
| Material Properties Transfer | No |
| CAD Associativity | Yes |
| Import Coordinate Systems | No |
| Reader Save Part File | No |
| Import Using Instances | Yes |
| Do Smart Update | No |
| Attach File Via Temp File | Yes |
| Temporary Directory | C:\Documents and Settings\ENB229.FOREST.005\Application Data\Ansys\v120 |
| Analysis Type | 3-D |
| Mixed Import Resolution | None |
| Enclosure and Symmetry Processing | Yes |

**Table 8 - Model (B4, C4, D4) > geometry > parts**

| Object Name | *substrate* | *film* |
|---|---|---|
| State | Meshed | |
| **Graphics Properties** | | |
| Visible | Yes | |
| Transparency | 1 | |
| **Definition** | | |
| Suppressed | No | |
| Stiffness Behavior | Flexible | |
| Coordinate System | Default Coordinate System | |
| Reference Temperature | By Environment | |
| **Material** | | |
| Assignment | Si | W |
| Nonlinear Effects | Yes | |
| Thermal Strain Effects | Yes | |
| **Bounding Box** | | |
| Length X | 5.e-002 m | |
| Length Y | 0.8 m | |
| Length Z | 4.e-002 m | 9.9998e-005 m |
| **Properties** | | |
| Volume | 1.6e-003 m³ | 4.e-006 m³ |
| Mass | 3.728 kg | 7.7e-002 kg |
| Centroid X | 0. m | |
| Centroid Y | 0. m | |
| Centroid Z | -2.e-002 m | -4.005e-002 m |
| Moment of Inertia Ip1 | 0.19932 kg·m² | 4.1068e-003 kg·m² |
| Moment of Inertia Ip2 | 1.2737e-003 kg·m² | 1.6042e-005 kg·m² |
| Moment of Inertia Ip3 | 0.1996 kg·m² | 4.1228e-003 kg·m² |
| **Statistics** | | |
| Nodes | 8799 | 3228 |
| Elements | 1600 | 400 |
| Mesh Metric | None | |

***Appendix A (Continued)***

*Coordinate Systems*

**Table 9 - Model (B4, C4, D4) > coordinate system**

| | |
|---|---|
| Object Name | *Global Coordinate System* |
| State | Fully Defined |
| **Definition** | |
| Type | Cartesian |
| Ansys System Number | 0. |
| **Origin** | |
| Origin X | 0. m |
| Origin Y | 0. m |
| Origin Z | 0. m |
| **Directional Vectors** | |
| X Axis Data | [ 1. 0. 0. ] |
| Y Axis Data | [ 0. 1. 0. ] |
| Z Axis Data | [ 0. 0. 1. ] |

*Connections*

**Table 10 - Model (B4, C4, D4) > connections**

| | |
|---|---|
| Object Name | *Connections* |
| State | Fully Defined |
| **Auto Detection** | |
| Generate Contact On Update | Yes |
| Tolerance Type | Slider |
| Tolerance Slider | 0. |
| Tolerance Value | 2.0064e-003 m |
| Face/Face | Yes |
| Face/Edge | No |
| Edge/Edge | No |
| Priority | Include All |
| Group By | Bodies |
| Search Across | Bodies |
| Revolute Joints | Yes |
| Fixed Joints | Yes |
| **Transparency** | |
| Enabled | Yes |

**Table 11 - Model (B4, C4, D4) > connections > contact region**

| | |
|---|---|
| Object Name | *Bonded - substrate To film* |
| State | Fully Defined |
| **Scope** | |
| Scoping Method | Geometry Selection |
| Contact | 1 Face |
| Target | 1 Face |

| | |
|---|---|
| Contact Bodies | substrate |
| Target Bodies | film |
| **Definition** | |
| Type | Bonded |
| Scope Mode | Manual |
| Behavior | Symmetric |
| Suppressed | No |
| **Advanced** | |
| Formulation | Pure Penalty |
| Normal Stiffness | Program Controlled |
| Update Stiffness | Never |
| Thermal Conductance | Program Controlled |
| Pinball Region | Program Controlled |

*Mesh*

**Table 12 - Model (B4, C4, D4) > mesh**

| | |
|---|---|
| Object Name | *Mesh* |
| State | Solved |
| **Defaults** | |
| Physics Preference | Mechanical |
| Relevance | 0 |
| **Sizing** | |
| Use Advanced Size Function | On: Fixed |
| Relevance Center | Coarse |
| Initial Size Seed | Active Assembly |
| Smoothing | Medium |
| Transition | Fast |
| Min Size | Default (4.0003e-004 m) |
| Max Face Size | 1.e-002 m |
| Max Tet Size | Default (8.0006e-002 m) |
| Growth Rate | Default (1.850 ) |
| Minimum Edge Length | 1.e-004 m |
| **Inflation** | |
| Use Automatic Tet Inflation | None |
| Inflation Option | Smooth Transition |
| Transition Ratio | 0.272 |
| Maximum Layers | 5 |
| Growth Rate | 1.2 |
| Inflation Algorithm | Pre |
| View Advanced Options | No |
| **Advanced** | |
| Shape Checking | Standard Mechanical |
| Element Midside Nodes | Program Controlled |
| Straight Sided Elements | No |
| Number of Retries | 0 |
| Rigid Body Behavior | Dimensionally Reduced |
| Mesh Morphing | Disabled |

| Pinch | |
|---|---|
| Pinch Tolerance | Default (3.6002e-004 m) |
| Generate on Refresh | No |
| **Statistics** | |
| Nodes | 12027 |
| Elements | 2000 |
| Mesh Metric | None |

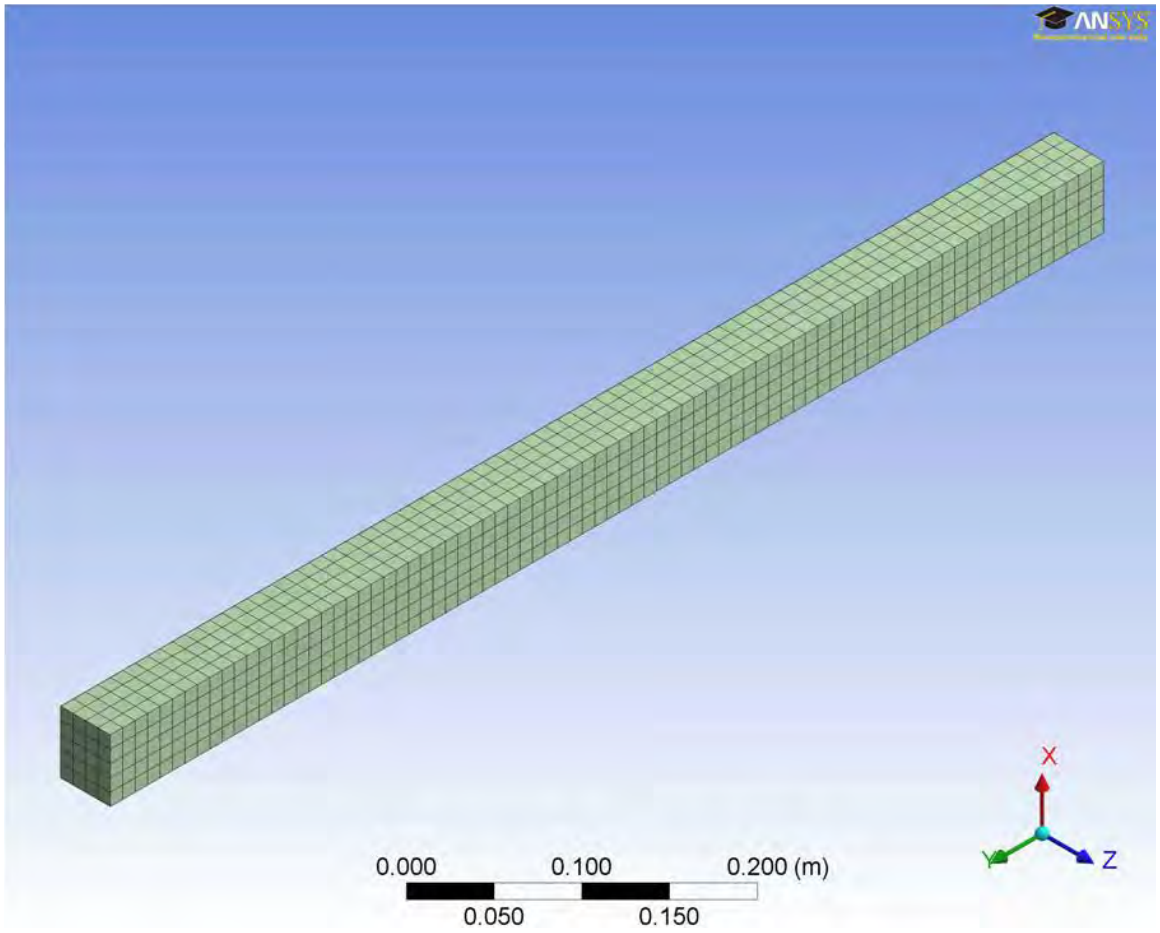


**Figure 34 - Showing mesh**

*Named Selections*

**Table 13- Model (B4, C4, D4) > named selections > named selections**

| Object Name | *all* |
|---|---|
| State | Fully Defined |
| **Definition** | |
| Send to Solver | Yes |
| Visible | Yes |
| **Scope** | |
| Geometry | 2 Bodies |

| Statistics | |
|---|---|
| Type | Manual |
| Total Selection | 2 Bodies |
| Suppressed | 0 |
| Hidden | 0 |

*Steady-State Thermal (B5)*

**Table 14 - Model (B4, C4, D4) > analysis**

| | |
|---|---|
| Object Name | *Steady-State Thermal (B5)* |
| State | Solved |
| **Definition** | |
| Physics Type | Thermal |
| Analysis Type | Steady-State |
| Solver Target | ANSYS Mechanical |
| **Options** | |
| Generate Input Only | No |

**Table 15 - Model (B4, C4, D4) > steady-state thermal (B5) > initial condition**

| | |
|---|---|
| Object Name | *Initial Temperature* |
| State | Fully Defined |
| **Definition** | |
| Initial Temperature | Uniform Temperature |
| Initial Temperature Value | 22. °C |

**Table 16 - Model (B4, C4, D4) > steady-state thermal (B5) > analysis settings**

| | |
|---|---|
| Object Name | *Analysis Settings* |
| State | Fully Defined |
| **Step Controls** | |
| Number Of Steps | 1. |
| Current Step Number | 1. |
| Step End Time | 1. s |
| Auto Time Stepping | Program Controlled |
| **Solver Controls** | |
| Solver Type | Program Controlled |
| **Nonlinear Controls** | |
| Heat Convergence | Program Controlled |
| Temperature Convergence | Program Controlled |
| Line Search | Program Controlled |
| **Output Controls** | |
| Calculate Thermal Flux | Yes |
| Calculate Results At | All Time Points |

*Appendix A (Continued)*

| Analysis Data Management | |
|---|---|
| Solver Files Directory | E:\THESIS\Ansyssimulation\091710_files\dp0\SYS\MECH\ |
| Future Analysis | None |
| Scratch Solver Files Directory | |
| Save ANSYS db | No |
| Delete Unneeded Files | Yes |
| Nonlinear Solution | No |
| Solver Units | Active System |
| Solver Unit System | mks |

**Table 17 - Model (B4, C4, D4) > steady-state thermal (B5) > loads**

| Object Name | *Temperature* | *Heat Flow* |
|---|---|---|
| State | Fully Defined | Suppressed |
| **Scope** | | |
| Scoping Method | Geometry Selection | |
| Geometry | 1 Face | |
| **Definition** | | |
| Type | Temperature | Heat Flow |
| Magnitude | 26.5 °C (ramped) | 43. W (ramped) |
| Suppressed | No | Yes |
| Define As | | Heat Flow |

*Appendix A (Continued)*

**Table 18 - Model (B4, C4, D4) > steady-state thermal (B5) > commands (ANSYS)**

```
!   Commands inserted into this file will be executed just prior to the
Ansys SOLVE command.
!   These commands may supersede command settings set by Workbench.

!   Active UNIT system in Workbench when this object was created:
Metric (m, kg, N, s, V, A)


*SET,_FNCNAME,'x091310'
*SET,_FNCCSYS,0
! /INPUT,F:\THESIS\Ansyssimulation\091310.func,,,1
*DIM,%_FNCNAME%,TABLE,6,23,1,,,,%_FNCCSYS%
!
! Begin of equation: (472400+400000*EXP(-
(125000*{X}^2+10.33*{Y}^2)))*EXP
! (2000*{Z})
*SET,%_FNCNAME%(0,0,1), 0.0, -999
*SET,%_FNCNAME%(2,0,1), 0.0
*SET,%_FNCNAME%(3,0,1), 0.0
*SET,%_FNCNAME%(4,0,1), 0.0
*SET,%_FNCNAME%(5,0,1), 0.0
*SET,%_FNCNAME%(6,0,1), 0.0
*SET,%_FNCNAME%(0,1,1), 1.0, -1, 0, 0, 0, 0, 0
*SET,%_FNCNAME%(0,2,1), 0.0, -2, 0, 1, 0, 0, -1
*SET,%_FNCNAME%(0,3,1),   0, -3, 0, 1, -1, 2, -2
*SET,%_FNCNAME%(0,4,1), 0.0, -1, 0, 2, 0, 0, 2
*SET,%_FNCNAME%(0,5,1), 0.0, -2, 0, 1, 2, 17, -1
*SET,%_FNCNAME%(0,6,1), 0.0, -1, 0, 125000, 0, 0, -2
*SET,%_FNCNAME%(0,7,1), 0.0, -4, 0, 1, -1, 3, -2
*SET,%_FNCNAME%(0,8,1), 0.0, -1, 0, 2, 0, 0, 3
*SET,%_FNCNAME%(0,9,1), 0.0, -2, 0, 1, 3, 17, -1
*SET,%_FNCNAME%(0,10,1), 0.0, -1, 0, 10.33, 0, 0, -2
*SET,%_FNCNAME%(0,11,1), 0.0, -5, 0, 1, -1, 3, -2
*SET,%_FNCNAME%(0,12,1), 0.0, -1, 0, 1, -4, 1, -5
*SET,%_FNCNAME%(0,13,1), 0.0, -2, 0, 1, -3, 3, -1
*SET,%_FNCNAME%(0,14,1), 0.0, -1, 7, 1, -2, 0, 0
*SET,%_FNCNAME%(0,15,1), 0.0, -2, 0, 400000, 0, 0, -1
*SET,%_FNCNAME%(0,16,1), 0.0, -3, 0, 1, -2, 3, -1
*SET,%_FNCNAME%(0,17,1), 0.0, -1, 0, 472400, 0, 0, -3
*SET,%_FNCNAME%(0,18,1), 0.0, -2, 0, 1, -1, 1, -3
*SET,%_FNCNAME%(0,19,1), 0.0, -1, 0, 2000, 0, 0, 4
*SET,%_FNCNAME%(0,20,1), 0.0, -3, 0, 1, -1, 3, 4
*SET,%_FNCNAME%(0,21,1), 0.0, -1, 7, 1, -3, 0, 0
*SET,%_FNCNAME%(0,22,1), 0.0, -3, 0, 1, -2, 3, -1
*SET,%_FNCNAME%(0,23,1), 0.0, 99, 0, 1, -3, 0, 0
! End of equation: (900000+50000000*EXP(-
(125000*{X}^2+10.33*{Y}^2)))*EXP(2000*
! {Z})
!-->
! LGWRITE,'091310','lgw','F:\thesis\Ansyssimulation\',COMMENT
bf,all,hgen,%x091310%
```

***Appendix A (Continued)***

*Solution (B6)*

**Table 19 - Model (B4, C4, D4) > steady-state thermal (B5) > solution**

| Object Name | *Solution (B6)* |
|---|---|
| State | Solved |
| **Adaptive Mesh Refinement** | |
| Max Refinement Loops | 1. |
| Refinement Depth | 2. |

**Table 20 - Model (B4, C4, D4) > steady-state thermal (B5) > solution (B6) > solution information**

| Object Name | *Solution Information* |
|---|---|
| State | Solved |
| **Solution Information** | |
| Solution Output | Solver Output |
| Update Interval | 2.5 s |
| Display Points | All |

**Table 21 - Model (B4, C4, D4) > steady-state thermal (B5) > solution (B6) > results**

| Object Name | *Temperature* |
|---|---|
| State | Solved |
| **Scope** | |
| Scoping Method | Geometry Selection |
| Geometry | All Bodies |
| **Definition** | |
| Type | Temperature |
| By | Time |
| Display Time | Last |
| Calculate Time History | Yes |
| Identifier | |
| **Results** | |
| Minimum | 26.5 °C |
| Maximum | 26.793 °C |
| Minimum Occurs On | substrate |
| Maximum Occurs On | substrate |
| **Information** | |
| Time | 1. s |
| Load Step | 1 |
| Substep | 1 |
| Iteration Number | 1 |

*Appendix A (Continued)*

**Table 22 - Model (B4, C4, D4) > steady-state thermal (B5) > solution (B6) > probes**

| | |
|---|---|
| Object Name | *Reaction Probe* |
| State | Solved |
| **Definition** | |
| Type | Reaction |
| Location Method | Boundary Condition |
| Boundary Condition | Temperature |
| **Options** | |
| Display Time | End Time |
| **Results** | |
| Heat | -38.043 W |
| **Maximum Value Over Time** | |
| Heat | -38.043 W |
| **Minimum Value Over Time** | |
| Heat | -38.043 W |
| **Information** | |
| Time | 1. s |
| Load Step | 1 |
| Substep | 1 |
| Iteration Number | 1 |

***Appendix A (Continued)***

*Transient Thermal (C5)*

**Table 23 - Model (B4, C4, D4) > analysis**

| | |
|---|---|
| Object Name | *Transient Thermal (C5)* |
| State | Solved |
| **Definition** | |
| Physics Type | Thermal |
| Analysis Type | Transient |
| Solver Target | ANSYS Mechanical |
| **Options** | |
| Generate Input Only | No |

**Table 24 - Model (B4, C4, D4) > transient thermal (C5) > initial condition**

| | |
|---|---|
| Object Name | *Initial Temperature* |
| State | Fully Defined |
| **Definition** | |
| Initial Temperature | Non-Uniform Temperature |
| Initial Temperature Environment | Steady-State Thermal |
| Time | End Time |

**Table 25 - Model (B4, C4, D4) > transient thermal (C5) > analysis settings**

| | |
|---|---|
| Object Name | *Analysis Settings* |
| State | Fully Defined |
| **Step Controls** | |
| Number Of Steps | 1. |
| Current Step Number | 1. |
| Step End Time | 110. s |
| Auto Time Stepping | Program Controlled |
| Initial Time Step | 1.1 s |
| Minimum Time Step | 0.11 s |
| Maximum Time Step | 11. s |
| Time Integration | On |
| **Solver Controls** | |
| Solver Type | Program Controlled |
| **Nonlinear Controls** | |
| Heat Convergence | Program Controlled |
| Temperature Convergence | Program Controlled |
| Line Search | Program Controlled |
| Nonlinear Formulation | Program Controlled |
| **Output Controls** | |
| Calculate Thermal Flux | Yes |
| Calculate Results At | All Time Points |

| Analysis Data Management | |
|---|---|
| Solver Files Directory | E:\THESIS\Ansyssimulation\091710_files\dp0\SYS-1\MECH\ |
| Future Analysis | None |
| Scratch Solver Files Directory | |
| Save ANSYS db | No |
| Delete Unneeded Files | Yes |
| Nonlinear Solution | No |
| Solver Units | Active System |
| Solver Unit System | mks |

**Table 26 - Model (B4, C4, D4) > transient thermal (C5) > loads**

| Object Name | *Temperature 2* |
|---|---|
| State | Fully Defined |
| **Scope** | |
| Scoping Method | Geometry Selection |
| Geometry | 1 Face |
| **Definition** | |
| Type | Temperature |
| Magnitude | 34. °C (step applied) |
| Suppressed | No |

*Solution (C6)*

**Table 27 - Model (B4, C4, D4) > transient thermal (C5) > solution**

| Object Name | *Solution (C6)* |
|---|---|
| State | Solved |
| **Adaptive Mesh Refinement** | |
| Max Refinement Loops | 1. |
| Refinement Depth | 2. |

**Table 28 - Model (B4, C4, D4) > transient thermal (C5) > solution (C6) > solution information**

| Object Name | *Solution Information* |
|---|---|
| State | Solved |
| **Solution Information** | |
| Solution Output | Solver Output |
| Update Interval | 2.5 s |
| Display Points | All |

*Appendix A (Continued)*

**Table 29 - Model (B4, C4, D4) > transient thermal (C5) > solution (C6) > solution information > result charts**

| Object Name | *Temperature - Global Maximum* | *Temperature - Global Minimum* |
|---|---|---|
| State | Solved | |
| **Scope** | | |
| Scoping Method | Global Maximum | Global Minimum |
| **Definition** | | |
| Type | Temperature | |
| **Results** | | |
| Minimum | 34. °C | 26.622 °C |
| Maximum | 34. °C | 33.995 °C |

**Table 30 - Model (B4, C4, D4) > transient thermal (C5) > solution (C6) > results**

| Object Name | *Temperature* |
|---|---|
| State | Solved |
| **Scope** | |
| Scoping Method | Geometry Selection |
| Geometry | All Bodies |
| **Definition** | |
| Type | Temperature |
| By | Time |
| Display Time | 76.653 s |
| Calculate Time History | Yes |
| Identifier | |
| **Results** | |
| Minimum | 33.961 °C |
| Maximum | 34. °C |
| Minimum Occurs On | film |
| Maximum Occurs On | substrate |
| **Minimum Value Over Time** | |
| Minimum | 26.622 °C |
| Maximum | 33.995 °C |
| **Maximum Value Over Time** | |
| Minimum | 34. °C |
| Maximum | 34. °C |
| **Information** | |
| Time | 76.653 s |
| Load Step | 1 |
| Substep | 18 |
| Iteration Number | 18 |

**Table 31 - Model (B4, C4, D4) > transient thermal (C5) > solution (C6) > probes**

| | |
|---|---|
| Object Name | *Heat Flux Probe* |
| State | Solved |
| **Definition** | |
| Type | Heat Flux |
| Location Method | Geometry Selection |
| Geometry | 1 Face |
| Orientation | Global Coordinate System |
| **Options** | |
| Result Selection | Z Axis |
| Display Time | 6.0237 s |
| Spatial Resolution | Use Maximum |
| **Results** | |
| Z Axis | 0.64973 W/m² |
| **Maximum Value Over Time** | |
| Z Axis | 2.2654 W/m² |
| **Minimum Value Over Time** | |
| Z Axis | 3.5898e-003 W/m² |
| **Information** | |
| Time | 1. s |
| Load Step | 1 |
| Substep | 1 |
| Iteration Number | 1 |

***Appendix A (Continued)***

*Static Structural (D5)*

**Table 32 - Model (B4, C4, D4) > analysis**

| | |
|---|---|
| Object Name | *Static Structural (D5)* |
| State | Solved |
| **Definition** | |
| Physics Type | Structural |
| Analysis Type | Static Structural |
| Solver Target | ANSYS Mechanical |
| **Options** | |
| Environment Temperature | 22. °C |
| Generate Input Only | No |

**Table 33 - Model (B4, C4, D4) > static structural (D5) > analysis settings**

| | |
|---|---|
| Object Name | *Analysis Settings* |
| State | Fully Defined |
| **Step Controls** | |
| Number Of Steps | 1. |
| Current Step Number | 1. |
| Step End Time | 1. s |
| Auto Time Stepping | Program Controlled |
| **Solver Controls** | |
| Solver Type | Program Controlled |
| Weak Springs | Program Controlled |
| Large Deflection | Off |
| Inertia Relief | Off |
| **Nonlinear Controls** | |
| Force Convergence | Program Controlled |
| Moment Convergence | Program Controlled |
| Displacement Convergence | Program Controlled |
| Rotation Convergence | Program Controlled |
| Line Search | Program Controlled |
| **Output Controls** | |
| Calculate Stress | Yes |
| Calculate Strain | Yes |
| Calculate Results At | All Time Points |
| **Analysis Data Management** | |
| Solver Files Directory | E:\THESIS\Ansyssimulation\091710_files\dp0\SYS-2\MECH\ |
| Future Analysis | None |
| Scratch Solver Files Directory | |
| Save ANSYS db | No |
| Delete Unneeded Files | Yes |
| Nonlinear Solution | No |
| Solver Units | Active System |
| Solver Unit System | mks |

**Table 34 - Model (B4, C4, D4) > static structural (D5) > imported load (setup)**

| Object Name | *Imported Load (Setup)* |
|---|---|
| State | Fully Defined |
| **Definition** | |
| Type | Imported Data |
| Interpolation Type | Mechanical Results Transfer |
| Suppressed | No |

**Table 35 - Model (B4, C4, D4) > static structural (D5) > imported load (setup) > imported body temperature**

| Object Name | *Imported Body Temperature* |
|---|---|
| State | Solved |
| **Scope** | |
| Scoping Method | Geometry Selection |
| Geometry | 2 Bodies |
| **Definition** | |
| Type | Imported Body Temperature |
| Suppressed | No |
| Source Environment | Steady-State Thermal (B5) |

*Solution (D6)*

**Table 36 - Model (B4, C4, D4) > static structural (D5) > solution**

| Object Name | *Solution (D6)* |
|---|---|
| State | Solved |
| **Adaptive Mesh Refinement** | |
| Max Refinement Loops | 1. |
| Refinement Depth | 2. |

**Table 37 - Model (B4, C4, D4) > static structural (D5) > solution (D6) > solution information**

| Object Name | *Solution Information* |
|---|---|
| State | Solved |
| **Solution Information** | |
| Solution Output | Solver Output |
| Newton-Raphson Residuals | 0 |
| Update Interval | 2.5 s |
| Display Points | All |

**Table 38 - Model (B4, C4, D4) > static structural (D5) > solution (D6) > results**

| | |
|---|---|
| Object Name | *Directional Deformation* |
| State | Solved |
| **Scope** | |
| Scoping Method | Geometry Selection |
| Geometry | All Bodies |
| **Definition** | |
| Type | Directional Deformation |
| Orientation | Z Axis |
| By | Time |
| Display Time | Last |
| Coordinate System | Global Coordinate System |
| Calculate Time History | Yes |
| Identifier | |
| **Results** | |
| Minimum | -2.1714e-007 m |
| Maximum | 3.0483e-007 m |
| Minimum Occurs On | film |
| Maximum Occurs On | substrate |
| **Information** | |
| Time | 1. s |
| Load Step | 1 |
| Substep | 1 |
| Iteration Number | 1 |

***Appendix A (Continued)***

*Material Data*

*Si*

**Table 39 - Si > constants**

| | |
|---|---|
| Density | 2330 kg m^-3 |
| Coefficient of Thermal Expansion | 2.6e-006 C^-1 |
| Thermal Conductivity | 149 W m^-1 C^-1 |
| Specific Heat | 710 J kg^-1 C^-1 |

**Table 40 - Si > isotropic elasticity**

| Temperature C | Young's Modulus Pa | Poisson's Ratio |
|---|---|---|
| | 1.85e+011 | 0.31 |

*W*

**Table 41 - W > constants**

| | |
|---|---|
| Density | 19250 kg m^-3 |
| Coefficient of Thermal Expansion | 4.5e-006 C^-1 |
| Thermal Conductivity | 173 W m^-1 C^-1 |
| Specific Heat | 131 J kg^-1 C^-1 |

**Table 42 - W > isotropic elasticity**

| Temperature C | Young's Modulus Pa | Poisson's Ratio |
|---|---|---|
| | 4.e+011 | 0.28 |